1983

Geological and thermal aspects of the southern San Joaquin Basin, California: application of the 40Ar/39Ar stepwise heating technique to detrital microclines

Kenneth Bé
University at Albany, State University of New York

Geological and thermal aspects of the southern San Joaquin Basin, California: application of the $^{40}Ar/^{39}Ar$ stepwise heating technique to detrital microclines

A thesis presented to the Faculty
of the State University of New York
at Albany
in partial fulfillment of the requirements
for the degree of
Master of Science

School of Arts and Sciences
Department of Geological Sciences

Kenneth Bé
1983

Geological and thermal aspects of the southern San Joaquin Basin, California: application of the $^{40}Ar/^{39}Ar$ stepwise heating technique to detrital microclines

Abstract of
a thesis presented to the Faculty
of the State University of New York
at Albany
in partial fulfillment of the requirements
for the degree of
Master of Science

School of Arts and Science
Department of Geological Sciences

Kenneth Bé
1983

Abstract

The depositional history of the southernmost region of the trough-shaped San Joaquin Basin spans from Upper Eocene to Recent time. The stratigraphy reveals both a predominantly marine environment which persisted until the Upper Pliocene, as well as nonmarine environments along the basin's margins. Folds and faults within the basin have resulted directly from movements along the San Andreas fault. Although the exact time of origin of the Big Bend is unclear, this major feature in the San Andreas fault's geometry has played an important role in recent crustal tectonics of southern California. Significantly, the southern San Joaquin's depocenter has undergone an acceleration in its rate of subsidence since late Pliocene time. Data on partial loss of radiogenic argon obtained from detrital microclines analyzed by $^{40}Ar/^{39}Ar$ stepwise heating technique provides information on temperatures experienced at various stratigraphic levels in the basin. The results agree with a thermal history predicted for the basin's recent and present rapid rate of subsidence.

Acknowledgements

I extend my sincerest thanks and appreciation to Dr. T. Mark Harrison for having introduced me to this field of research and especially for his generous devotion of time and patience to insure the success of my involvement in this project. I also thank Dr. Kevin Burke and Dr. John Delano for their many helpful comments and for consenting to be members of the committee reviewing this master's degree project. Samples were made available by Thane McCulloh, Nancy Naeser, and Charles Naeser of the U.S. Geological Survey. Robert Warasila and Robert Spangler provided minute-to-minute assistance guiding me through Stony Brook University's rare gas extraction and mass spectrometer system for two months of Summer '82. This research was supported financially by DOE grant DE-AC02-82ER13013.

Table of Contents

page

1. Introduction.....1

2. Sedimentation and Stratigraphy.....3

   2a. General setting.....3

   2b. Physiography.....6

   2c. Sedimentary sources.....7

   2d. Stratigraphy.....8

   2e. Sediment dispersal.....20

3. Structures and Tectonic Evolution.....23

   3a. Structures.....23

   3b. History of movement on the San Andreas fault system.....29

   3c. The Big Bend configuration of the San Andreas fault.....32

   3d. Transverse Ranges.....35

   3e. Sierra Nevada Block.....36

4. Summary.....37

References.....40

Appendix I: $^{40}Ar/^{39}Ar$ age apectrum analysis of detrital microclines from the southern San Joaquin Basin, California: an approach to determining the thermal evolution of sedimentary basins.....47

Appendix II: Tabulated data for the $^{40}Ar/^{39}Ar$ incremental heating runs of microcline separates from the Tejon and Basin Blocks.....90

Appendix III: Additional samples analyzed by the $^{40}Ar/^{39}Ar$ dating technique.....98

Figures

Figures 1a and 1b.....location maps

Figure 2.....diagrammatic summary of stratigraphy in the San Joaquin Basin

Figure 3.....isopach map for the Upper Eocene

Figure 4.....isopach map for the Oligocene

Figure 5.....isopach map for the Lower Miocene

Figure 6.....isopach map for the Middle Miocene

Figure 7.....isopach map for the Upper Miocene

Figure 8.....isopach map for the Pliocene

Figure 9.....sediment dispersal patterns during the Miocene

Figure 10.....major fold axes and faults, and subsurface structure contours in the San Joaquin Basin

Figure 11.....crustal movement vectors determined from the 1952 Arvin-Tehachapi earthquake

1. Introduction

Introduction

The purpose of this study was to determine the applicability of $^{40}Ar/^{39}Ar$ stepwise heating technique to detrital microclines from a sedimentary basin. By evaluating the partial loss, if any, of radiogenic argon from the microcline samples, it was predicted that meaningful quantitative data on the thermal history of the basin at different stratigraphic levels might be obtained from analyses of the samples. Although the technique has been successfully applied in prior work to terrestrial rock samples to determine original ages of cooling, only recently have thermal events been quantitatively evaluated using data on the amount of radiogenic argon loss from mineral samples.

The area chosen for study is the southernmost San Joaquin Basin in California. A previous study on fission track annealing experienced in apatites during burial in the basin yielded a well-constrained thermal history (Briggs and others, 1981). Light mineral concentrates from the suite of samples used in the fission track study were made available for the present study so that the results of the two experiments could be compared. It was also hoped that by using $^{40}Ar/^{39}Ar$ technique, an estimate on the timing of burial heating events might be obtained as well.

In addition to the advantage of a well understood thermal history, testing this technique on samples from the San Joaquin Basin was attractive due to the relatively straightforward depositional and structural history of the basin. Fairly continuous subsidence has occurred since the

deposition of the samples studied.

The first part of this thesis will review the stratigraphic and structural history of the southern San Joaquin Basin, and its tectonic evolution will be discussed in the context of interactions between the North American and Pacific plates during Neogene times. This information on the basin's geological history will provide a framework for the report on the results of the analyses of detrital microcline samples from the basin.

The second part (Appendix 1) describes the aims, method, principles, and modelling of the $^{40}Ar/^{39}Ar$ technique in its application to microcline crystals. This appendix appears in the final manuscript form of a paper in press in Earth and Planetary Science Letters, 1983, by T. M. Harrison and K. Be entitled "$^{40}Ar/^{39}Ar$ age spectrum analysis of detrital microclines from the southern San Joaquin Basin, California: An approach to determining the thermal evolution of sedimentary basins."

2. Sedimentation and Stratigraphy

Sedimentation and Stratigraphy

2a. General setting

The San Joaquin Valley occupies the southern half of the Great Valley in California, an elongate basin situated between the Sierra Nevada Range on the east and the Diablo and Temblor Ranges on the west side (see Figure 1). The northern subvalley is the Sacramento Valley. The two valleys are separated by a subsurface basement structural feature, the Stockton Arch, which traverses the Great Valley in an east to west direction. The areal extent of the San Joaquin Valley is approximately 390 km long and 65-80 km wide. The maximum thickness of sediment is estimated to be over 9100 m and is located in the southern San Joaquin Valley. In total, a volume of roughly 145,000 km^3 of sediment is contained within the San Joaquin basin. This sediment, all post-Jurassic in age, rests upon the gently west-dipping western flank of the Sierra Nevada metamorphic-plutonic basement complex. The west side of the basin is truncated abruptly by the San Andreas fault, where sedimentary units have been upturned and deformed. The San Joaquin Basin can be viewed as an asymmetric basin underlain by a homoclinal basement sloping westward from the Sierra Nevada Range and terminating abruptly along a steep western margin. Uplifted terranes bounding the southernmost margin of the San Joaquin Basin include the San Emigdio and Tehachapi Mountain Ranges. The shape and boundaries of the San Joaquin Valley appear to have remained virtually unchanged since late Miocene time

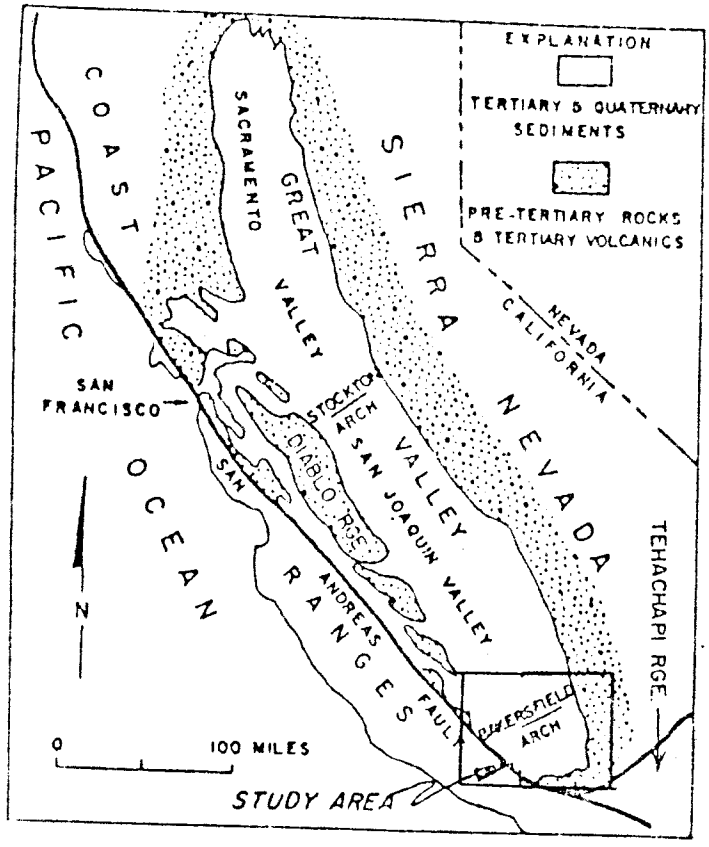

Figure 1a.

Major features in the
Great Valley of California.
(from MacPherson, 1978).

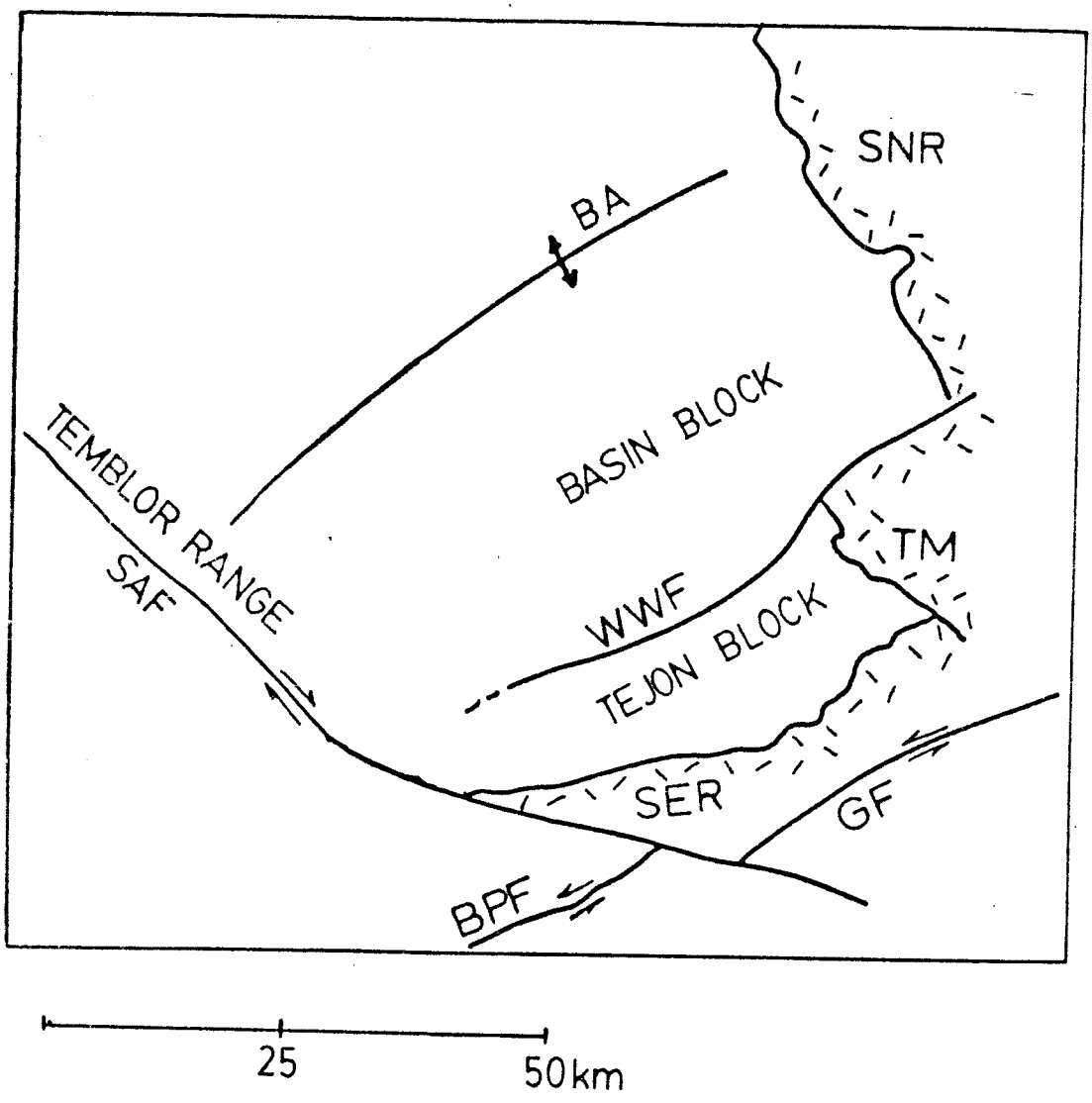

Figure 1b.

Major features of the southern San Joaquin Basin: SAF, San Andreas Fault; BPF, Big Pine Fault; GF, Garlock Fault; BA, Bakersfield Arch; WWF,White Wolf Fault; SNR, Sierra Nevada Range; TM, Tehachapi Mts.; SER, San Emigdio Range.

(Callaway, 1971).

The San Joaquin Basin can be divided further into two subbasins, the main San Joaquin Valley basin and the Maricopa subbasin. These two subdivisions lie to the north and south, respectively, of another major subsurface structural feature, the Bakersfield Arch. Since uplift of this arch appears to have started in late Paleocene or early Eocene times (MacPherson, 1978), the Neogene depositional history of the Maricopa subbasin can be treated separately from the rest of the San Joaquin basin.

It is the Maricopa subbasin which is the subject of the project dating the microcline samples using $^{40}Ar/^{39}Ar$ technique. For clarity, however, the Maricopa subbasin will be referred to simply as the "southern San Joaquin Basin". It should be noted that both names are frequently used in the relevant literature.

2b. Physiography

The southern San Joaquin basin is a valley of entirely interior drainage. Gently sloping alluvial fans and plains comprise most of the floor of the valley. At the valley's margins dissected, moderately tilted alluvial fans flank the foothills of the Sierra Nevada Range to the east and the Tehachapi and San Emigdio Ranges to the south. Large lakes occupied the central part of the valley during late Pleistocene time (Croft, 1968). Those in the southern San Joaquin Valley were the Buena Vista and Kern Lakes. These lakebeds, as well as the Tulare lakebed

to the north, are the sites where active tectonic subsidence has been maintained (Davis and Green, 1962). Other lacustrine depositional sites occupied topographic lows between anticlinal ridges.

2c. Sedimentary sources

Sedimentary source areas for the southern San Joaquin Basin include the southern Sierra Nevada Batholithic Range, Tehachapi Mountains, San Emigdio Range, and the Temblor Range. Because of displacement along the San Andreas fault, a formerly important sediment source terrane to the west of the basin has shifted in position to the northwest. This terrane, the Salinian Block, is revealed by thick accumulations of clasts and detritus along the western margin of the basin (Nilsen and Clarke, 1975).

The abundance of arkosic sediments indicates a richness of K-feldspar content in the source terranes. Underlying the source areas are: 1) granitic rocks 2) metamorphic rocks, including granitic gneisses, schists, quartzites, and metavolcanic rocks, 3) felsic to intermediate volcanic rocks, and, in lesser amounts, 4) sedimentary rocks, including sandstones, conglomerates, shales, mudstones, siltstones, and cherts. The uplifted sedimentary units forming the Temblor Range along the western San Joaquin margin would have provided the latter (Nilsen and Clarke, 1975). The San Emigdio and Tehachapi Ranges, uplifting since early Miocene times (Hackel, 1966), consist mainly of gneiss, schist, granitic and gabbroic rocks, and metasediments.

2d. Stratigraphy

The Great Valley contains sedimentary rocks ranging in age from Jurassic to Recent. Mesozoic rocks are thicker and more abundant in the Sacramento Basin and thin out over the Stockton Arch. Tertiary deposits, on the other hand, thicken south of the Stockton Arch and reach a maximum thickness in the western part of the southern San Joaquin Basin.

The Tertiary stratigraphy in the San Joaquin Basin is complex because of rapid, local changes in lithofacies units (Beck, 1965). Figure 2 shows a diagrammatic summary of the stratigraphy which lists the more important units in a single cross-section view from east to west. The following outline of the basin's stratigraphic history is compiled from reports by Hoots and others (1954), Simonson (1958), Hackel (1966), and Callaway (1971).

The sedimentary sequence in the San Joaquin Basin overlies a Mesozoic metamorphic and igneous basement. The eastern portion of the basement consists of metasediments, metavolcanics, and granites of the western flank of the Sierra Nevada Range. Westwards, the basement's petrology changes to a mafic or ultramafic composition. (Bailey and others, 1964).

No sedimentary strata in the southern San Joaquin Basin are known to predate the Upper Eocene. A major marine transgression, however, was responsible for depositing the oldest known sediment of Upper Eocene age in the southern San Joaquin Basin (see Figure 3). This sedimentary section, the Tejon Formation, consists of sandstone, siltstone, and

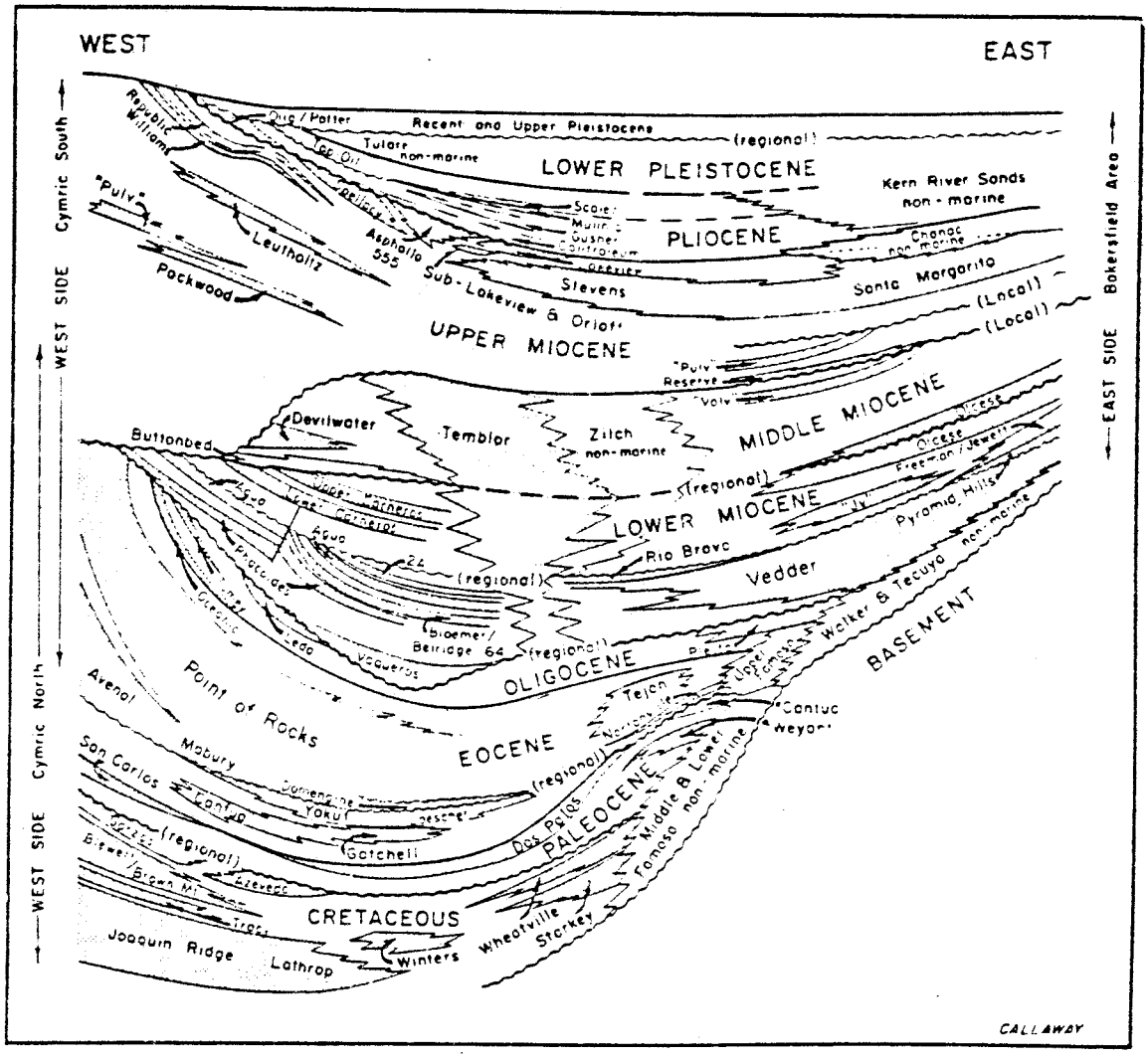

Figure 2. Diagrammatic summary of stratigraphic units in the San Joaquin Basin from east to west. (from Callaway, 1971).

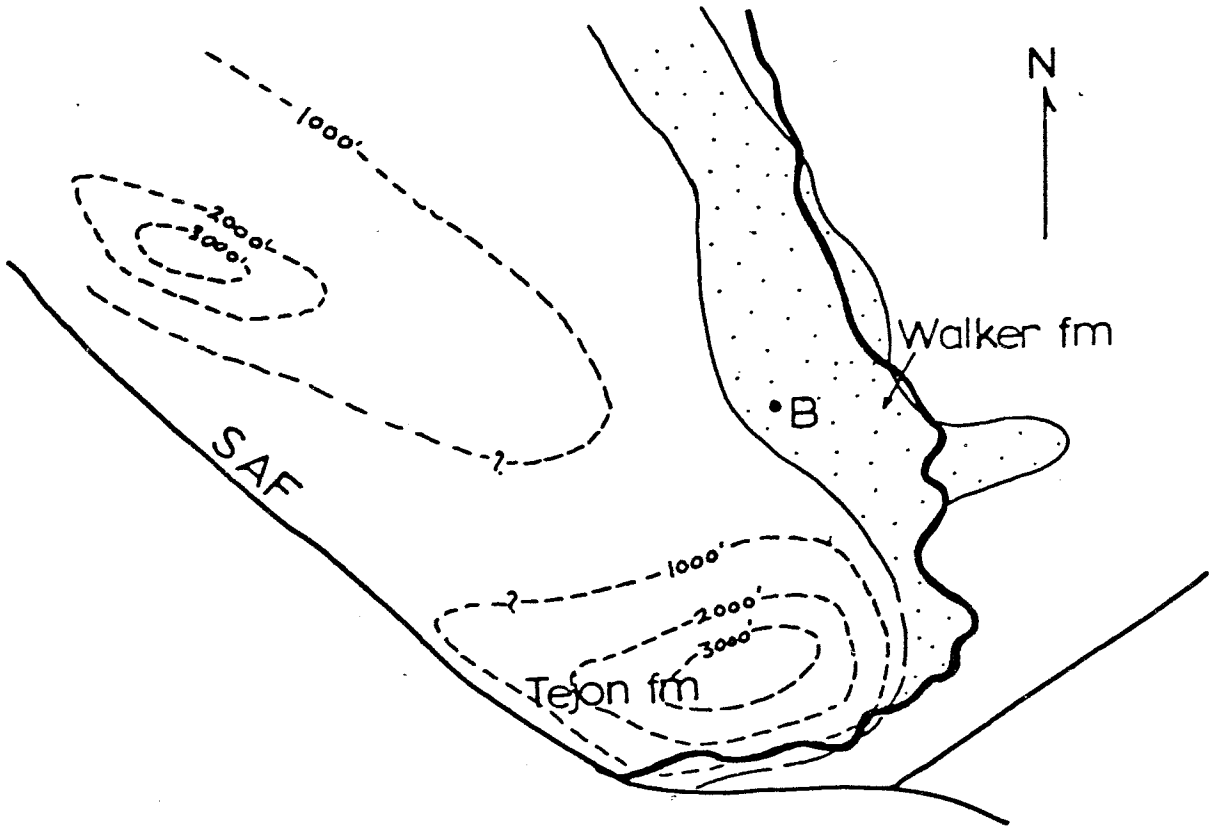

Figure 3. Isopach map for the Upper Eocene interval (modified from Hackel, 1966).

B = Bakersfield

SAF = San Andreas Fault

clay shale totalling 750 to 1300 m in thickness. The separation of the Tejon Formation from a time-equivalent conglomeratic sandstone called the Domengine Formation in the Bakersfield vicinity is the earliest evidence for the existence of the Bakersfield Arch as a depositional barrier. The Tejon Formation is indicative of a clastic sea and grades eastward into nonmarine continentally-derived clays and sands, collectively called the Walker Formation. The Walker Formation spans in age from Eocene to early Miocene.

A latest-Eocene to early Oligocene regional uplift event caused some erosion of Upper Eocene units and also a thinner deposition of Oligocene age sediments (Figure 4). Representing the Oligocene in the southern San Joaquin Basin are marine sandstones and siltstones of the San Emigdio Formation and lower section of the Pleito Formation. This unconformity overlain by marine units appears to correspond well to a major eustatic sea-level fall in the beginning of the Oligocene (see Vail and Hardenbol, 1979). Continental deposits of late Oligocene to early Miocene are were laid down at the extreme southeast of the basin (Tecuya Formation). Another erosional disconformity exists between Oligocene strata and the Miocene units above them.

During early Miocene time, the southern San Joaquin Basin was the only portion of the Great Valley which was inundated by the sea (Figure 5). The units deposited during this interval include the following from older to younger: the Silt Creek Shale, Phacoides Sandstone, Lower Santos Shale, Agua Sandstone, Upper Santos Shale, Carneros Sand-

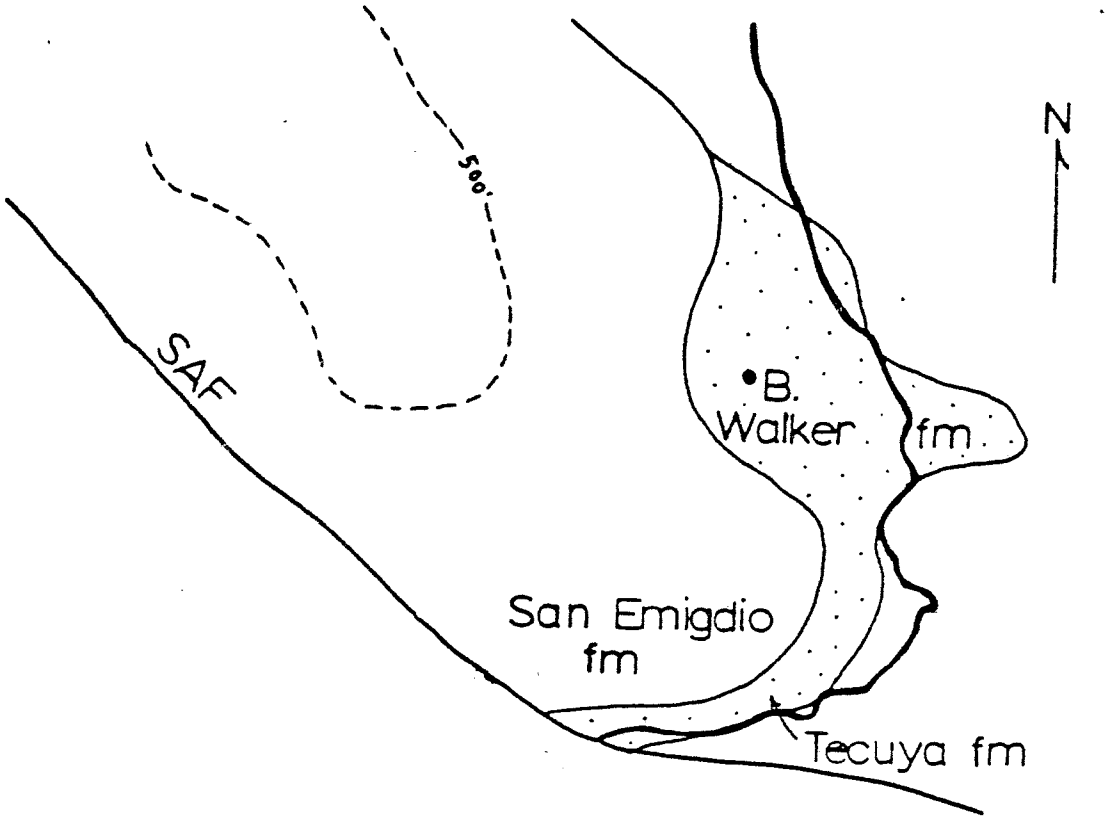

Figure 4. Isopach map for the Oligocene interval (modified from Hackel, 1966).

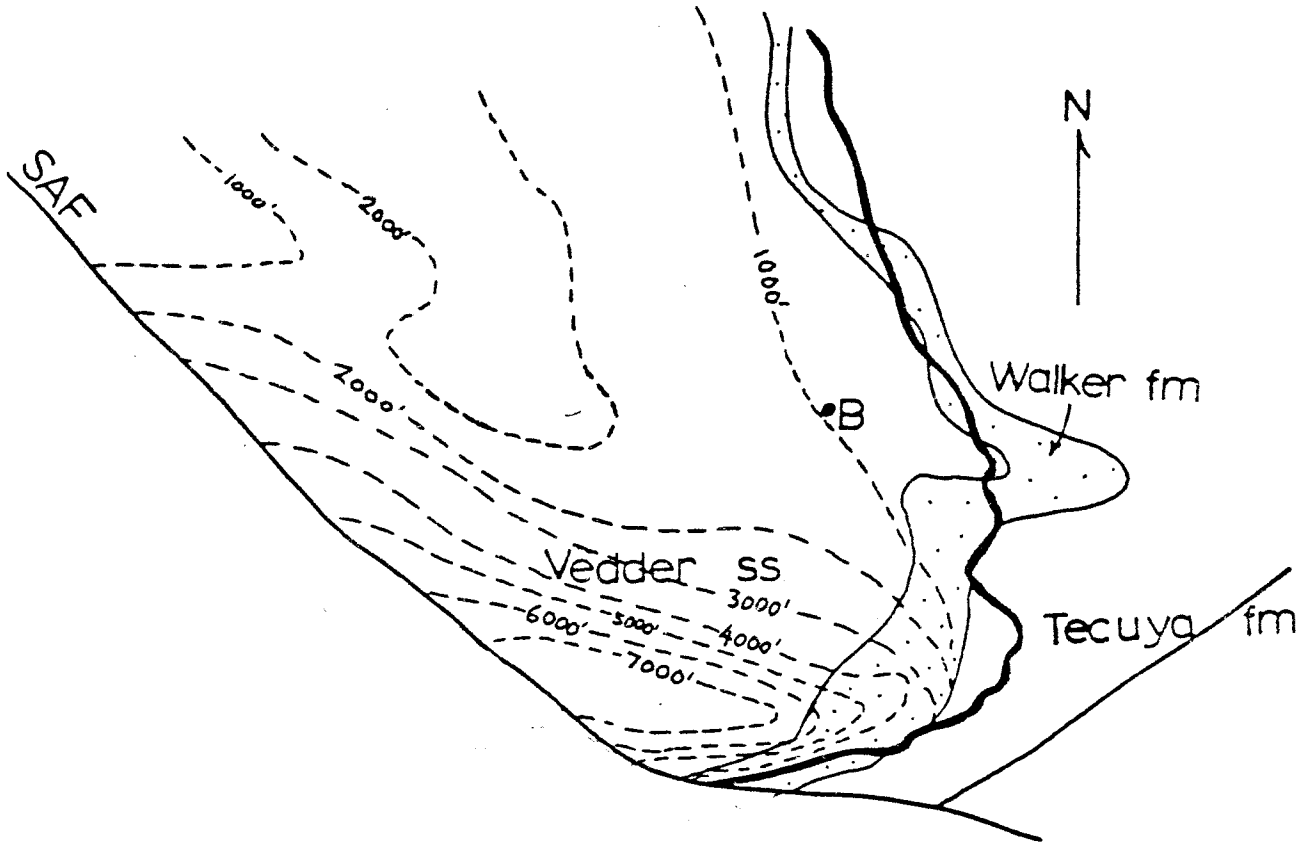

Figure 5. Isopach map for the Lower Miocene interval (modified from Hackel, 1966).

stone, and Media Shale all on the west side of the basin. The east side time-equivalent units are: the Vedder Formation, Pyramid Hill Sandstone, Jewett Siltstone, and the lower section of the Olcese Sandstone. The eastern nonmarine Walker and Tecuya Formations persisted as time-transgressive units into the early Miocene. It was during this interval that the Tehachapi Mountains and San Emigdio Range began to uplift. Igneous activity accompanying the uplift produced basaltic and dacitic flows at the southern margin of the basin, in addition to ash beds and bentonite deposits between stratigraphic horizons in the eastern part of the basin. Conglomerate beds distributed in the Lower Miocene sequence in the southwest part of the basin attest to the episodic rapid dispersal of sediment caused either by sporadic uplift of the source regions or sea-level changes, or a combination of both.

As in the Lower Miocene, marine deposition in the Great Valley during the Middle Miocene was limited to the southern half of the San Joaquin Basin (Figure 6). Middle Miocene sedimentary units from older to younger include: the Button Bed Sandstone, Gould Shale, and Devilwater Siltstone in the western part of the basin. The eastern part contains the Olcese Sandstone and Round Mountain Siltstone. Nonmarine sedimetns include the upper section of the Tecuya Formation and the Bena Gravels.

Transgression in the Great Valley increased the areal extent of marine sediment distribution during the late Miocene (Figure 7) and a greater variety of lithofacies

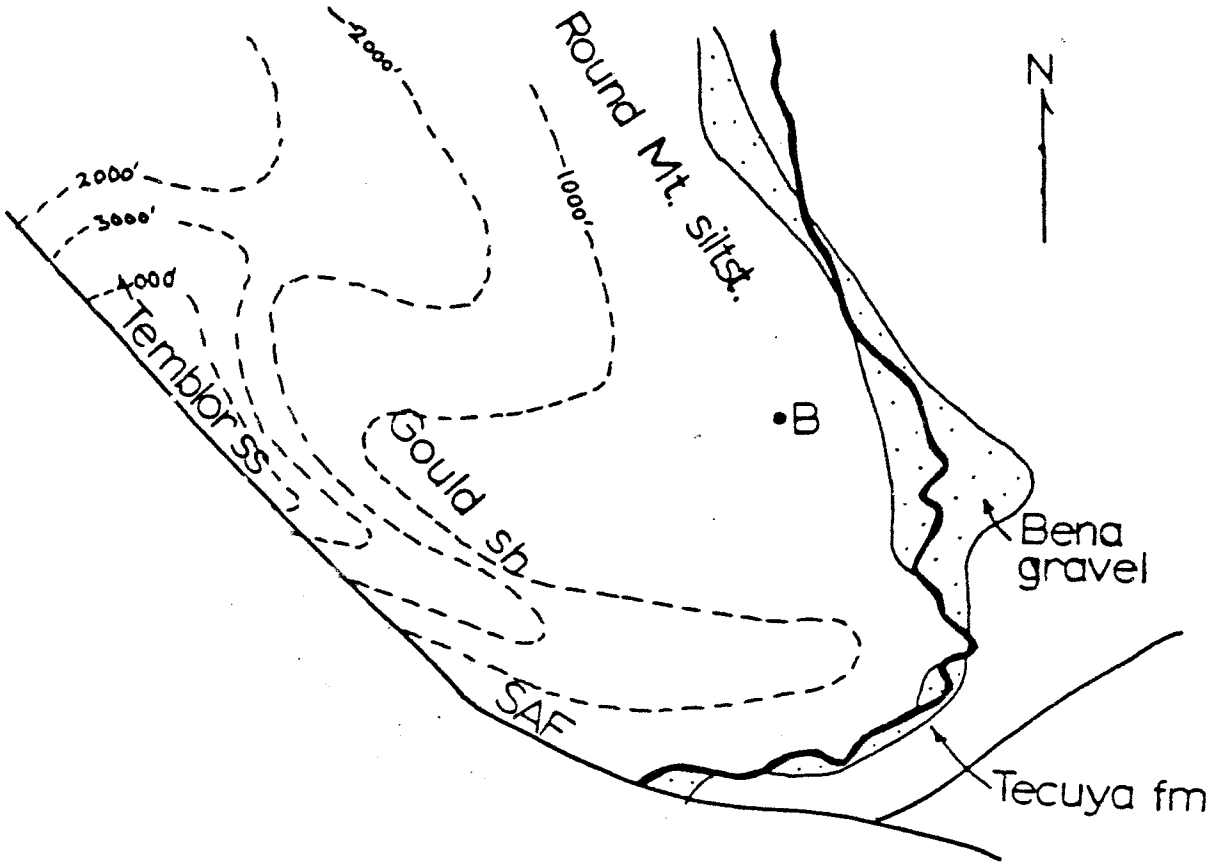

Figure 6. Isopach map for the Middle Miocene interval (modified from Hackel, 1966).

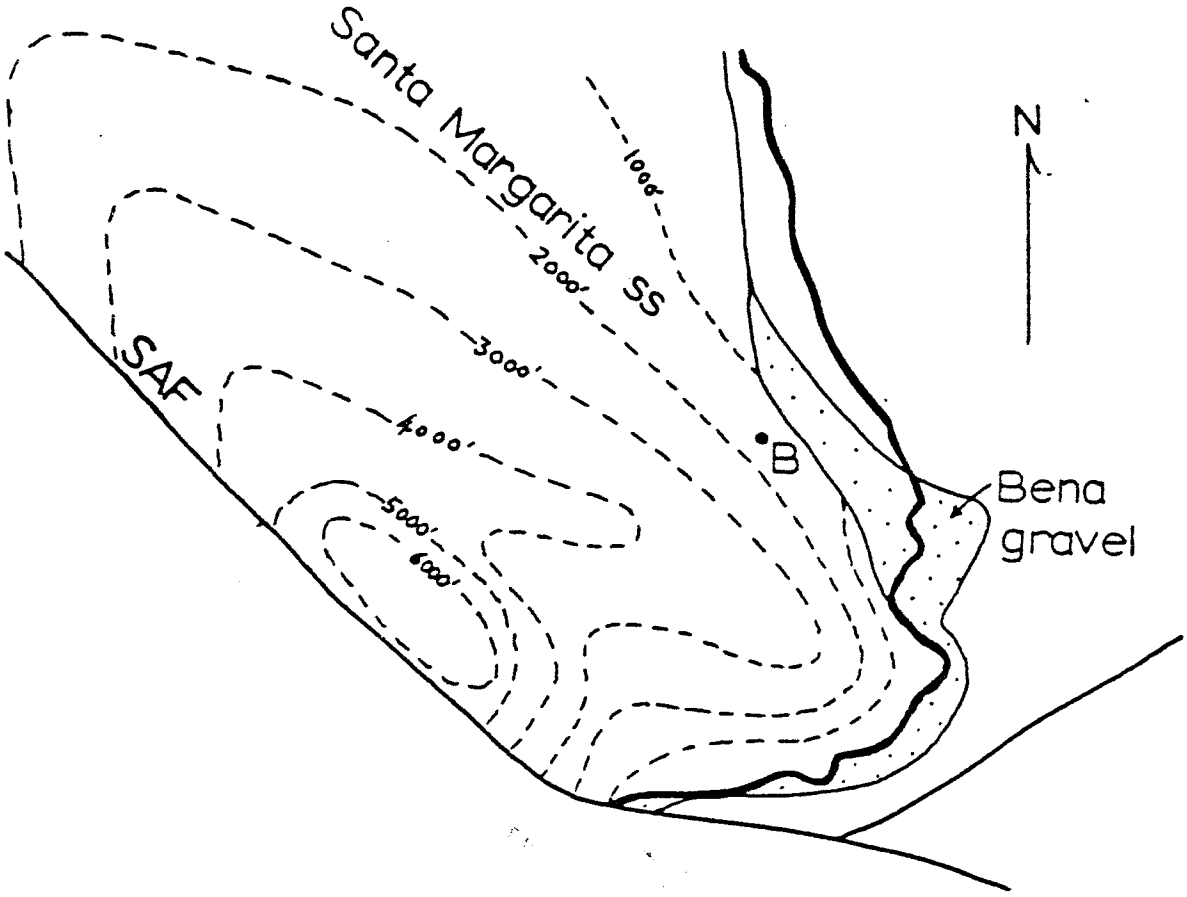

Figure 7. Isopach map for the Upper Miocene interval (modified from Hackel, 1966).

was formed during this time, particularly towards the west side. Although shales are predominant, rock types also include diatomite, chert, and conglomerates. Sandstones were abundantly deposited throughout the southern San Joaquin Basin through local channel transport, such as the Stevens and Santa Margarita Sandstones. Of the two contemporaneous units, the Santa Margarita represents shallower marine facies; towards the east it interfingers with the continentally-derived Bena Gravel, a marginal unit which continues from the middle Miocene. The large influx of nonmarine sand and clay accumulated in the southern San Joaquin Basin during the late Miocene (e.g., the lower section of the Chanac Formation) was a result of uplift along the eastern and southern margins of the basin. It is believed that the present configuration of the basin was established by this time interval.

Pliocene deposits (Figure 8) consist of both marine and nonmarine types. As in earlier times, the nonmarine deposits accumulated along the basin margins. They are represented by the Chanac and Kern River Formations along the east side, and in the west by the Tulare Formation. These nonmarine units are composed mostly of sandstones, conglomerates and claystones. Larger clast sizes are found closer to the source areas. Marine units, classified together as the Etchegoin Formation, are predominantly shales, sandstones, and conglomerates, reflecting a close proximity to the nonmarine lithofacies. Well over 1 km of sediment accumulated in the depocenter region of the southern San

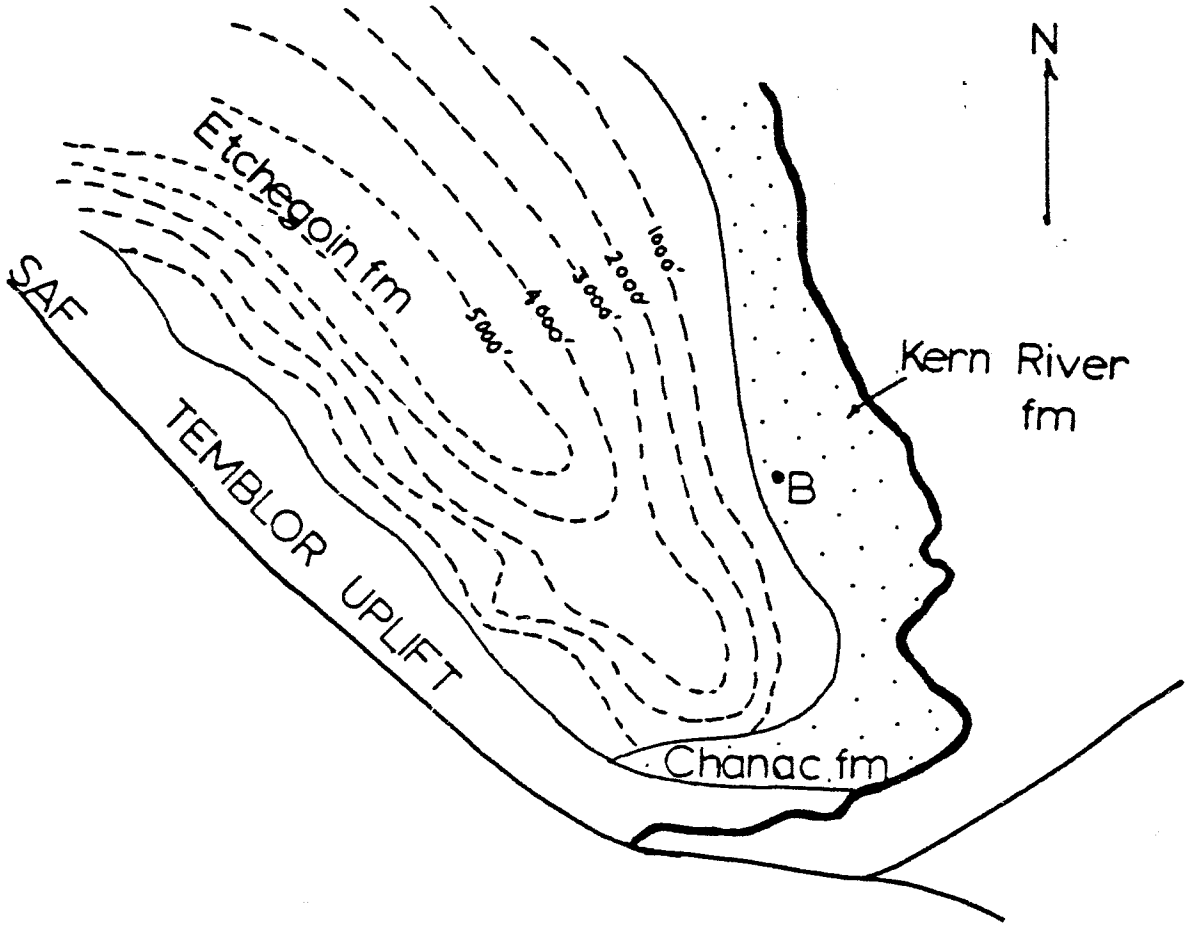

Figure 8. Isopach map for the Pliocene interval (modified from Hackel, 1966).

Joaquin Basin during the Pliocene interval.

Pleistocene to Recent deposits in the basin are entirely nonmarine. They appear to grade down into similarly nonmarine units of Pliocene age. The exact positions of the time-boundaries are hard to determine because of the lack of key fossils. The detritus in the coarse units indicate the source areas from which they were derived. Along the west side, the Tulare Formation consists of shales to pebble conglomerates eroded from the uplifted Temblor Range. The Kern River Formation to the east is composed of granitic sandstones and conglomerates derived from the Sierra Nevada Range. Similar to Pliocene time, sediment accumulation totals in excess of 1 km in the basin's depocenter.

The Pleistocene interval was the time of thickest accumulation in the southern San Joaquin Basin. Some suggestion will be made later about this sudden increase in subsidence and accumulation rates. First, however, it would be useful to discuss the modes of sediment dispersal, as well as the structural development within the basin, in order to understand how the basin evolved into its present form.

2e. Sediment dispersal

This discussion will be limited to well-documented time intervals of the basin's sedimentary history, particularly the Miocene since sandstones of that age have been the focus of detailed examination because of their potential as good petroleum reservoirs (Zieglar and Spotts, 1976). Studies by MacPherson (1978) and Webb (1981) provide detailed accounts of the mechanisms and nature of sediment dispersal in the basin during Miocene time. The abundance of recognizable turbidite units has made possible accurate paleoreconstructions of the sedimentation patterns.

It is important to note that depocenter locations and bathyal values underwent changes during the Oligocene through Pliocene history of the basin. Abyssal depths in excess of 2 km are recognized to have existed in Oligocene and Lower Miocene times based on foraminiferal paleoecologies (Bandy and Arnal, 1969). Rapid sedimentation which followed by Middle Miocene times succeeded in filling the basin sufficiently to decrease the depths to lower neritic types by late Miocene and Pliocene times. By comparing paleobathymetric and isopach data, it was found that the rates of deposition increased considerably in the later Miocene, as contrasted to roughly equivalent rates in subsidence and sedimentation in the Oligocene. In addition, this study showed that the depocenter in the southern San Joaquin Basin shifted progressively to the southeast by late Miocene time. thickening to a maxima near the San Andreas fault.

Marine clastic wedges identified as turbidite successions are well-documented in the basin (Webb, 1981). Known as the Stevens Sandstones, they consist of coarse, poorly-sorted quartzose to arkosic sandstones and occur interbedded with deep-water shales. These deposits derived from channels situated in troughs or canyons incised ito the basin margins. Channel patterns were controlled by compaction structures along the Bakersfield Arch and by anticlinal topography within the basin.

The channels originated from all directions around the basin, including the Bena channel (Bena Gravels) from the Sierra Nevada Range to the east, and channels stemming from the Tehachapi Mountains to the south and the newly-formed Temblor uplifts to the west. The ancestral Kern River, feeding sediment into the basin from a few kilometers east of Bakersfield was probably the principal source for the submarine fan deposits (MacPherson, 1978). Upon entering the basin floor though the canyons, the fans prograded westward in an arcuate fashion. Most notably, the turbidites were not confined to narrow, restricted zones. Instead, sediment dispersal was a wide-ranging, evenly-distributing process.

A reconstruction of turbidite dispersal patterns during the Miocene is shown in Figure 9. Of the the principal fans feeding the southern San Joaquin Basin, one of these, the Valpredo Fan is shown derived from the Tehachapi Mountains via transport over the newly-elevated Tejon Platform or Block.

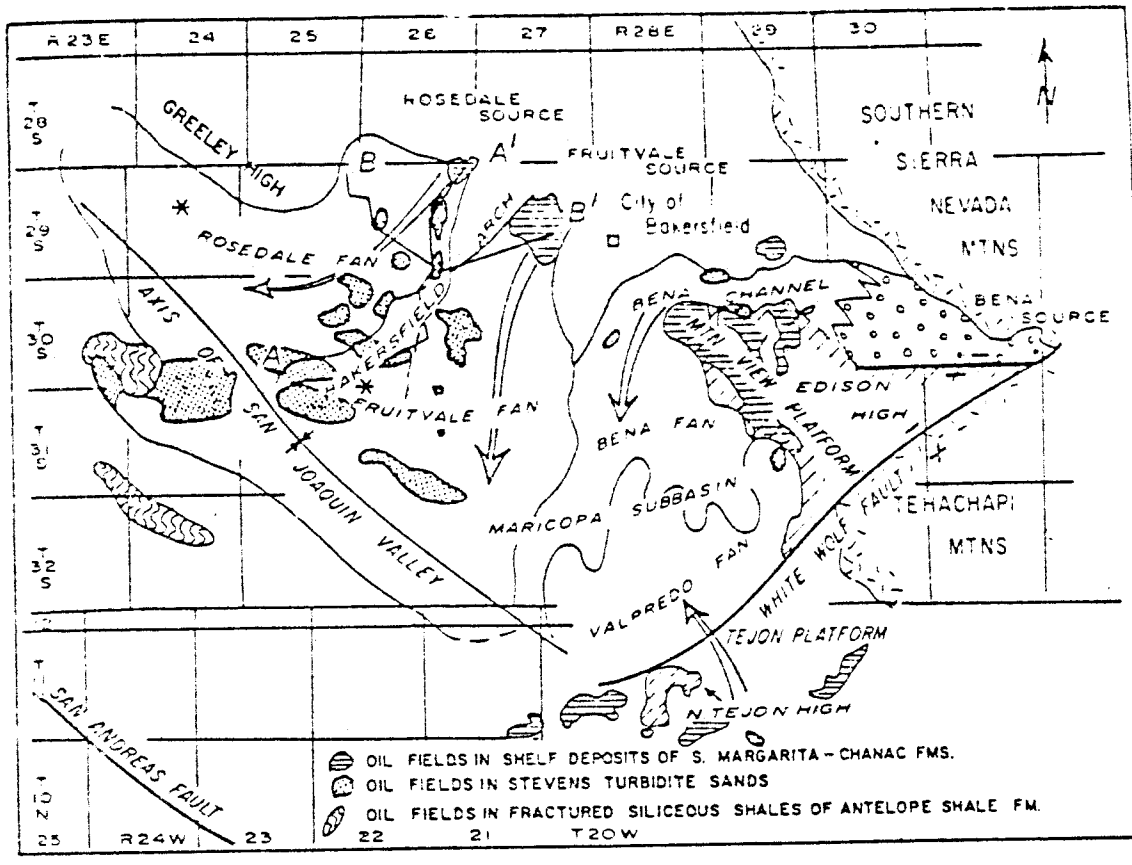

Figure 9. Sediment dispersal patterns during the Miocene (from MacPherson, 1978).

3. Structures and Tectonic Evolution

Structures and Tectonic Evolution

3a. Structures

Because of severe effects of the San Andreas fault system, the evolution of the southern San Joaquin Basin since early Miocene times is distinct from its earlier history of development. This fault system initiating during Oligocene time (Atwater and Molnar, 1973), probably truncated and deformed western marginal stratigraphic units and influenced the formation of a complex array of en echelon folds within the basin. More recently, the change of the fault's geometry into a more west-oriented bend has resulted in active thrusting along the southern margin of the basin.

Knowledge of the basin's subsurface structure is especially important for understanding the processes of petroleum accumulation. In basins cut-through or bounded by a strike-slip fault the locations of drag folds and secondary folds can be predicted (Moody, 1973) . Hardy (1976) located and defined a distinct set of anticlines using subsurface well-log data in the San Joaquin Basin. The anticlines are tightly folded, traversed by numerous faults at high angles to their anticlinal trend, and for the most part concentrated along the western, fault-bounded region of the basin (Figure 10). All the anticlines trend to the northwest and are typical 'right-stepping' patterns, conforming to the right-slip motion of the San Andreas fault. Regionally, this anticlinorium along the basin's western margin comprises the Temblor Range.

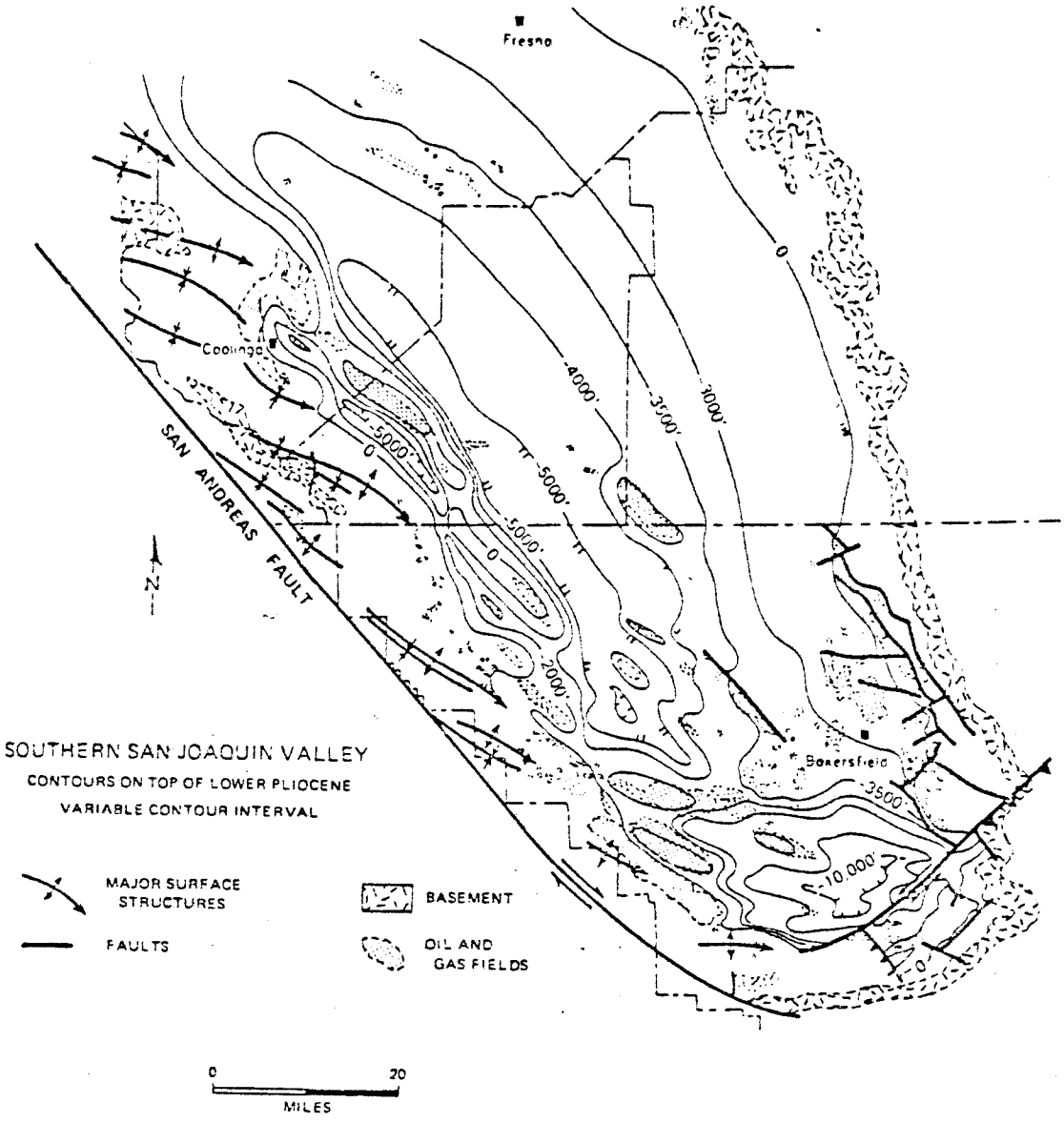

Figure 10. Major fold axes and faults, and subsurface structure contours in the San Joaquin Basin (from Harding, 1976).

The northwestern end of the range contains a core of Cretaceous rocks flanked by exposures of Paleocene to Pleistocene sediments (Karp, 1968), whereas only Tertiary strata have been uplifted and eroded through in the southeast Temblors in the vicinity of the southern San Joaquin Basin. Wheeler Ridge is one of the major anticlines in the southwesternmost San Joaquin Valley which contains sediments of Pliocene to Quaternary age (Cunningham, 1926), now uplifted to a peak elevation of 500 m above the valley floor.

The en echelon pattern of anticlines was formed synchronously with the sequence of strike-slip movement on the San Andreas fault (Harding, 1976). Comparison of deformed and undeformed subsurface strata indicates that the earliest folding began in early Miocene time. This observation accords with a model proposing renewed movement on the San Andreas fault at about this time following a stage of apparent quiescence during the Oligocene (see below). Also observed is that folding occurred more extensively in the basin by the late Miocene in response to a notable increase in the rate of slip on the San Andreas fault.

Harding (1976) also distinguished two distinct cases in the sequential growth of the anticlinorium. In some anticlines older strata at greater depth showed a marked increase in the degree of flexure as a result of several stages of flexing affecting the anticline. In other cases, anticlines were observed to have terminated in growth while more basinward strata began to deform to create young-

er anticlines. In this latter case, it is difficult to envisage how folding should continue basinward while separated from an active strike-slip fault zone by a zone of non-deforming strata. Recent data strongly indicates the presence of a major fault trending parallel to the San Andreas system in the center of the San Joaquin Basin (A. Sylvester, pers. comm., 1983). This may explain one reason for the basinward propagation of folding.

Apart from those faults which cross-cut the anticlines, other faults are present in the basin. The eastern margin of the San Joaquin Valley is dominated by apparent normal faulting which has disrupted Miocene and youner sediments (Fox, 1929). It is, however, possible that some amount of horizontal offset has also occurred since shear displacement in the western United Staes is known to involve a wide zone (Livaccari, 1979).

The southwestern part of the San Joaquin Valley contains low-angle thrusts (collectively, the Pleito Thrust) consisting of mid-Tertiary strata which have been carried northwards over younger basin strata (Crowell, 1975). The Pleito Thrust is a recent manifestation of transpression in the region of the San Andreas fault immediately to the south (Crowell, 1964).

An active, oblique-slip fault trending east-northeast traverses the central part of the southern San Joaquin Basin. The sense of movement on this fault, called the White Wolf fault, is well-known from seismic data obtained during a major earthquake which occurred along the fault

in 1952 (Richter scale magnitude 7.7, see Benioff, 1955a). The aftershock sequence showed that strain rebound on the southeast side of the fault was generated by compressional strains, while the northwest side of the fault was characterized by rebound from shear strain (Benioff, 1955a) Further analysis of the seismicity indicated that a component of overthrusting to the northwest on a plane dipping about 60-70 degrees to the southeast (Båth and Richter, 1958; Scheidegger, 1959). Figure 11 illustrates the directions of crustal movement observed from the 1952 Arvin-Tehachapi earthquake.

Over 3 km of vertical displacement has been inferred for the White Wolf fault since Pliocene time (Dibblee, 1955). Since the time of its inception in the late Pliocene, the major effect of this fault on the evolution of the southern San Joaquin Basin has been the division of the basin into two distinct blocks, the Basin block and Tejon block. The Basin block and Tejon block. The Basin block, also known as the Maricopa depocenter (see Figure 1) has undergone an accelerated rate of subsidence since the late Pliocene. Uplift of the Tejon block has been maintained up to recent times and continues to affect the pattern of sedimentation as noted earlier.

The existence of the White Wolf fault was virtually unnoticed before the 1952 earthquake. Its position, orientation, and sense of movement suggest that it relieves highly concentrated stress generated by the apparently anomalous high-angle intersection of the left-slipping Garlock with the San Andreas fault, as well as the bend in the San

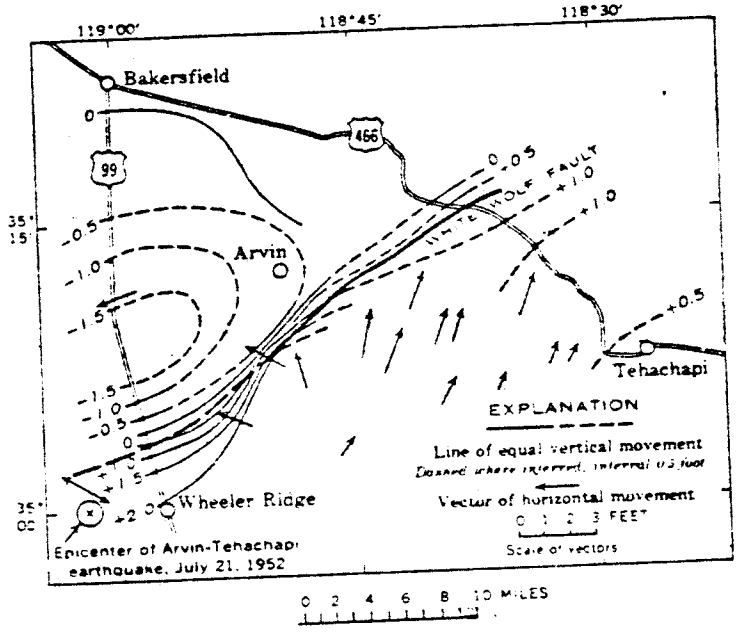

Figure 11. Crustal movement vectors determined from the 1952 Arvin-Tehachapi earthquake (from Lofgren, 1965).

Andreas (Benioff, 1955b). The kinematics of this zone of the San Andreas system are critical in the post-Pliocene history of the basin and will be discussed following a review of movement history along the San Andreas fault.

3b. History of movement on the San Andreas fault system

The San Andreas fault is believed to have had two main stages of development, the first occurring during late-Cretaceous through Paleocene time totalling about 300 km of right-slip displacement and the second, initiating in Early Miocene-Upper Oligocene time, contributing an additional 300 km to produce a total of about 600 km of offset (Crowell, 1979).

Evidence for latest-Cretaceous to Paleocene displacement is indicated by sedimentary units derived from a source terrane which is believed to be presently about 560 km to the southeast on the eastern side of the fault (Ross and others, 1973).

Approximately 320 km of offset has been proposed for units of middle and late Eocene ages (Nilsen and Dibblee, 1974 ; Clarke and Nilsen, 1973). The relatively small amount of offset determined for these units compared with an almost equal amount (300 km) for early Miocene rocks is cited as evidence supporting the hypothesis that a period of quiescence in fault movement occupied the post-Pliocene to early Miocene interval (Huffman, 1972; Dickinson and others, 1972; Nilsen and Clarke, 1975).

The rejuvenation of movement is indicated by early Miocene volcanic rocks dated at 22 Ma old and upper Oligocene rocks 23.5 Ma in age, both which have been displaced approximately 300 km (Turner and others, 1970).

It has also been inferred that movement occurred elsewhere during this interval of quiescence along the modern fault system. This inferred movement is believed to have been accomodated by a "proto-San Andreas" fault for which no direct geologic evidence can be found at present (Suppe, 1970). Therefore, the modern San Andreas fault probably developed by late Miocene time subparallel to older fault systems which variably displaced slivers of the western North American margin (Howell, 1975).

The second stage of fault movement since early Miocene time fits predictions which result from the plate interactions modelled by Atwater (1970) and Atwater and Molnar (1973). Based on ocean-floor magnetic anomaly interpretations, relative movements between the Pacific and North American plates were studied for the intervals between 38, 29, 21.2, 10, 4.5, and 0 Ma ago. The reconstructions indicate that the spreading ridge which separated the Pacific and Farallon plates came into contact with the western margin of the North American plate at aroun 29 Ma ago. This event initiated a northward-migrating ridge-transform-trench junction and a southward-migrating ridge-trench-transform junction. Resulting from this dynamic configuration was an increasing length of right-lateral shear along the western North American

plate. The initiation of a strike-slip boundary at about 29 Ma ago was responsible for the starting of basin formation in western California and offshore Baja at that time (Blake and others, 1978; Nilsen and Clarke, 1975).

The reconstruction by Atwater and Molnar (1973) also calculated an acceleration in the rate of movement between the two plates from 29 Ma ago to the present. Averages of the rates of right-slip show an increase from 1.3 cm/yr between 21 and 10 Ma ago to 4 cm/yr between 10 to 4.5 Ma ago. Since 4.5 Ma ago, the average rate has increased further to approximately 5.5 cm/yr. Blake and others (1978) reported changes in the azimuth of shear of about 16 degrees between the Pacific and North American plates during these three time intervals. The data show an azimuth shift from a more northerly to a more westerly orientation. This effect is considered to be an important factor influencing the inception of Neogene basins in offshore northern and central California (Blake and others, 1978). The low precision of this data, however, limits the value of this interpretation.

The Neogene history of the San Andreas fault is highly relevant to the development of the southern San Joaquin Basin's structural features as already stated.

A zone of subparallel faults is necessary to account for the total amount of displacement between the Pacific and North American plates, only sixty percent of which has been accomodated by the present day San Andreas fault (Graham and Dickinson, 1972). During interaction of the

plates, a complex tectonic evolution has occurred within zones of subparallel faults (e.g., San Andreas, San Gabriel, Elsinore, San Jacinto faults) involving squeezing, stretching, and rotation of crustal fragments (Freund, 1974; Crowell, 1979; Sylvester and Darrow, 1979; Luyendyk and others, 1980). The Salinian block, a key former source terrane for the early San Joaquin Basin was deformed by such slivering and extension by subparallel faults (Johnson and Normark, 1974).

The faults and fault splays themselves have also been rotated, one such example being the San Gabriel fault. This fault is assumed to have been rotated as well as abandoned around 4 Ma ago (Crowell, 1975). Right-lateral movement continued along the present straight segment of the San Andreas fault northwest of the San Gorgonio Pass. This location is immediately south along the fault from the well-known "Big Bend", the topic of the next section.

3c. The Big Bend configuration of the San Andreas fault

The southern end of the San Joaquin Basin displays abundant evidence of a strongly compressional environment. Presently active concentration of compressional stress in this region is evident from careful measurements of marker displacements. The Tehachapi Mountains have been observed to be flexing upward in the central part of the range and coupled with uplift of the Tejon block (Lofgren, 1965). An approximately 0.3×10^{-6}/yr of uniaxial north-south contraction was observed in southern California over a six year interval (Savage and others, 1979).

The acceleration of subsidence in the southern San Joaquin Basin over the past 4 to 7 Ma is a result of adjustments in the larger-scale tectonics in the region (Yeats, 1978; Page, 1982). The concentration of compressive stress in this vicinity is due to the "Big Bend" configuration in the San Andreas fault. This segement of the fault trends anomalously in a nearly east-west orientation between Tejon and San Gorgonio Pass. Movement along the San Andreas fault is essentially "locked" in the Big Bend region (Allen, 1968).

Other faults, such as the San Gabriel fault, in southern California having a similar trend orientation are presently inactive faults, indicating the highly unstable condition of this geometry. The San Gabriel, once a major part of the San Andreas system, was rotated into its present orientation and abandoned when right-lateral movement was taken up along a nearby , northwest-oriented fault (Crowell, 1979). It therefore appears that the Big Bend is a transient feature.

The initial cause of development of the Big Bend has been attributed to the opening of the Gulf of California roughly 5 Ma ago (Chase and others, 1970; Henyey, 1976; Page, 1982). At about this time, the San Andreas system is inferred to have made a rapid transition to a more inland location to connect with the northeast part of the new spreading center in the Gulf of California (Livaccari, 1979).

A serious space consideration exists in the Big Bend region where the Garlock and Big Pine faults join the San Andreas (see Figure 1). These two secondary faults are both left-lateral in motion and join the San Andreas system at an angle of about fourty degrees. Offset on the Big Pine fault initially involved dip-slip motion in the early Miocene, but since the late Miocene has totalled about 13-15 km of left slip (Hill and Dibblee, 1953; Dibblee, 1976). Crustal compression has occurred in the wedged region between the Big Pine and San Andreas faults, where abundant east-west folds have formed (Crowell, 1964).

The Garlock fault has undergone about 65 km of left-lateral displacement (Davis and Burchfiel, 1973). This fault has been considered to be a major intra-continental transform fault which evolved from different crustal extension rates between the Basin and Range province to the northeast and the Mojave block to the south (Hamilton and Meyers, 1966; Davis and Burchfiel, 1973).

The Mojave Desert is a crustal block situated between the Garlock and San Andreas faults. East-trending folds and strike-slip faults indicate the deformation experienced in this block from north-south compression (Garfunkel, 1974; Cummings, 1976).

The crustal space problem posed by the junction of the San Andreas, Garlock, and Big Pine faults is that the convergence of crust is apparently occurring from all directions. Thrusting towards the north and south of the Big Bend is, in part, able to accomodate this convergence.

It has also been proposed that the Big Bend configuration itself evolved only recently from the position of the two active left-lateral faults by the San Andreas system to their present locations (Bohannon and Howell, 1982).

3d. Transverse Ranges

The misalignment between the orientation of the Big Bend and direction of shear vectors is also believed to be responsible for maintaining uplift in the Transverse Ranges immediately to the south (Jahns, 1973; Hill, 1982). The Transverse Ranges form a prominent east-west structural trend at a high angle to the main trend of the San Andreas fault. Seismic and gravity observations indicate that the Transverse Ranges lack a deeply-rooted isostatic support, so it is probable that tectonically-generated compressional stresses maintain uplift (Hadley and Kanamori, 1977). The Transverses are still uplifting actively at present (Castle and others, 1976).

Studies of basins within the Transverse Ranges indicate complicated histories since Miocene time (Jahns, 1973). East-trending basins formed by crustal extension in the Miocene were later shortened and overridden by marginal thrusts by Pliocene time. One explanation for the reorientation of stresses in the Transverse region may be that the crustal block as a whole underwent counterclockwise rotation, as indeed paleomagnetic measurements have shown (Kammerling and Luyendyk, 1977). Models of rigid, fault-bounded blocks in a right-lateral megashear

zone have demonstrated geometrically how the rotation of crustal units is necessary to accomodate the large magnitude of shear displacement between the Pacific and North American plates during the Neogene (Luyendyk and others, 1980).

3e. Sierra Nevada block

The Sierra Nevada block has also experienced some displacement due to shear deformation during the Neogene. Paleomagnetic evidence has shown a fifty percent clockwise deflection in the southern Sierra Nevada with an inclination of twenty degrees from the value expected, a configuration which appears to predate the early Miocene (Kanter and McWilliams, 1980). This data would also support a hypothesis proposing displacement of the Sierra Nevada block during the active interval of the inferred proto-San Andreas fault (Hay, 1976).

4. Summary

4. Summary

The southern San Joaquin Basin is the location a thick sedimentary depocenter which has experienced an acceleration in subsidence rate during the late Neogene. The sediments have been derived from uplifted basement and deformed strata surrounding the southern portion of the Great Valley. Because of movement along the San Andreas fault, the major western sedimentary source terrane has been displaced to the northwest. Other source terranes, such as the Tehachapi Mountains to the south, appear to have been major sediment contributors only since early Miocene times. In comparison, the Sierra Nevada Range has continually supplied the entire Great Valley with sediment since the late Mesozoic.

The sediments, which range in age from Upper Eocene to Recent, consist primarily of sandstones and shales. The stratigraphic pattern is complex in detail, but in general trends from deeper marine in the western part of the basin to shallow marine and continentally-derived in the east and south. Thick continentally-derived clastic wedges were deposited by local channel streams derived from the surrounding uplands. Abrupt lithofacies changes reflect the rapid adjustment of the channels to variable uplift in the source terranes and to subsidence in the basin. Since Pliocene time, the basin ceased to contain a marine environment and has received a steady influx of continentally-derived clastic sediments. Until

most recently, lakes occupied the central valley floor.

The sedimentation rate has generally kept in equilibrium with the rate of subsidence, although in pre-middle Miocene times, abyssal depths were maintained by a more rapid rate of subsidence.

The structural features in the southern San Joaquin Basin are characteristic of wrench fault tectonic zones. En echelon anticlinal folding is consistent with right-slip along the San Andreas fault. This indicates a range of structural growth histories. Faults occupy all parts of the basin. The anticlines are typically cross-cut by secondary faults. The western margin displays apparent normal fault displacement with downthrown blocks basinward. The southwesternmost margin of the basin is overridden by low-angle thrusts. The White Wolf fault is a major oblique left-slip fault which divides the basin into its present configuration consisting of the Basin and Tejon Blocks.

Intense deformation in the southern San Joaquin Basin, as well as the increased rate of subsidence since the Pliocene is caused by transpression in the Big Bend region of the San Andreas fault. The exact origin and timing of this feature is poorly-understood, but may be closely-related to the connection of the San Andreas system with the newly-opened Gulf of California rift about 5 Ma ago. Other major tectonic features involved in the structural complexity of the Big Bend region include the

left-lateral Garlock and Big Pine faults, Transverse Ranges, Mojave Desert, and southern Sierra Nevada Range. Overall, the present dynamic aspects of the southern San Joaquin Basin are the result of the highly unstable concentration of compressive stress in this region.

References

Allen, C.R. (1968), The tectonic environments of seismically active and inactive areas along the San Andreas Fault: Stanford Univ. Publ. geol. Sci. 11, p.70-83.

Allen, C.R., P. St. Armand, C.F. Richter, and J.M. Nordquist (1965), Relationship between seismicity and geologic structure in the southern California region (San Joaquin County): Seismol. Soc. America Bull., v. 55, no. 4, p. 753-798.

Atwater, T. (1970), Implications of plate tectonics for the Cenozoic tectonic evolution of western North America: Geol. Soc. America Bull., v.81, p.3513-3536.

Atwater, T. and P. Molnar (1973), Relative motion of the Pacific and North American plates deduced from seafloor spreading in the Atlantic, Indian, and South Pacific Oceans: in Proceedings of the conference on tectonic problems of the San Andreas fault system, Stanford Univ. Publ. geol. Sci., v.13,, p.136-148.

Bailey, E.M., W.P. Irwin, and D.L. Jones (1964), Franciscan and related rocks and their significance in the geology of western California: Calif. Div. Mines and Geology Bull. 183, 177pp.

Ballance, P.F. (1980), Models of sediment distribution in nonmarine and shallow marine environments in oblique-slip fault zones: in Sedimentation in Oblique-Slip Mobile Zones (Ballance, P.F., and H.G. Reading, eds.), Spec. Publ. int. Assoc. Sediment., v.4, p.229-236.

Bandy, O.L., and A.E. Arnal (1969), Middle Tertiary basin development, San Joaquin Valley, California: Geol. Soc. America Bull., v.80, p.783-820.

Barbat, W.F. (1947), Stratigraphy of San Joaquin Valley (abstr.): Oil and Gas Jour., v.45, n.47, p.128.

Båth, M. and C.F. Richter (1958), Mechanisms of aftershocks of the Kern County, California, earthquake of 1952: Seismol. Soc. America Bull., v.48, no.2, p.133-146.

Beck, R.E. (1965), Biostratigraphic highlights of some deep wells from the central southern San Joaquin Valley (Kings County) (abstr.): Amer. Assoc. Petrol. Geol. Bull., v.49, no.7, p.1079.

Benioff, H. (1955a), Mechanisms and strain characteristics of the White Wolf fault as indicated by the aftershock sequence: Calif. Div. Mines and Geology Bull.,

v.171, p.199-202.

Benioff, H. (1955b), Relation of the White Wolf fault to the regional tectonic pattern: Calif. Div. Mines and Geology Bull., v.171, p.203-204.

Blake, M.C., Jr., R.H. Campbell, T.W. Dibblee, Jr., D.G. Howell, T.H. Nilsen, W.R. Normark, J.C. Vedder, and E.A. Silver (1978), Neogene basin formation in relationship to plate-tectonic evolution of San Andreas fault system, California: Amer. Assoc. Petrol. Geol. Bull., v.62, no.3, p. 344-372.

Bohannon, R.G., and D.G. Howell (1982), Kinematic evolution of the San Andreas, Garlock, and Big Pine faults, California: Geology, v.10, p.358-363.

Briggs, N.D., C.W. Naeser, and T.H. McCulloh (1981), Thermal history of sedimentary basins by fission-track dating: Nuclear Tracks, v.5, p.235-237.

Burchfiel, B.C., and G.A. Davis (1981), Mojave desert and environs: in The Geotectonic Development of California (Ernst, W.G., ed.), Prentice-Hall, Englewood Cliffs, N.J., 1981, 706pp.

Buwalda, J.P. (1954), Geology of the Tehachapi Mountains, California: Calif. Div. Mins and Geology Bull., v.170, p.131-142.

Callaway, D.C. (1971), Petroleum Potential of the San Joaquin Basin, California: in Future Petroleum Provinces of the United States - their Geology and Potential (Cram, I.H., ed), Amer. Assoc. Petrol. Geol., 1971, p.239-253.

Castle, R.O., J.P. Church, and M.R. Elliot (1976), Aseismic uplift in southern California: Science, v.192, p.251-253.

Chase, C.G., H.W. Menard, R.L. Larsen, G.F. Sharman, and S.M. Smith (1970), History of sea-floor spreading west of Baja California: Geol. Soc. America Bull., v.81, p.491-497.

Christensen, M.N. (1966), Late Cenozoic crustal movement in the Sierra Nevada of California: Geol. Soc. America Bull., v.77, p.163-182.

Clarke, S.H., Jr., and T.H. Nilsen (1973), Displacement of Eocene strata and implications for the history of offset along the San Andreas fault, central and northern California: in Conference on tectonic problems of the San Andreas fault system, Proc., Stanford Univ. Publ.

Geol Sci., v.13, p.358-367.

Croft, M.G. (1968), Geology and radiocarbon ages of late Pleistocene lacustrine clay deposits, southern part of the San Joaquin Valley, California: in Geological Survey Research, 1968, Chap. B, U.S. Geol. Survey Prof. Paper 600-B, p.B151-156.

Crowell, J.C. (1974), Origin of late Cenozoic basins in southern California: in Tectonics and Sedimentation (Dickinson, W.R., ed.), Soc, Econ. Paleontologists and Mineralogists Spec. Publ. 22, 204pp., p.190-202.

Crowell, J.C. (1975a), The San Andreas Fault in southern California: in San Andreas Fault in Southern California (Crowell, J.C., ed.), Calif. Div. Mines and Geology Spec. Report 118, 272pp.

Crowell, J.C. (1979), The San Andreas fault system through time: Jour. Geol. Soc. London, v.136, p.293-302.

Cummings, D. (1970), Theory of plasticity applied to faulting, Mojave Desert, southern California: Geol. Soc. America Bull., v.87, p.720-724,

Cunningham, G.M. (1926), The Wheeler Ridge oil field (Kern County): Amer. Assoc. Petrol. Geol. Bull., v.10, no.5, p.495-501.

Davis, G.A., and D.C. Burchfiel (1973), Garlock fault: an intracontinental transform structure, southern California: Geol. Soc. America Bull., v.84, p.1407-1422.

Davis, G.H., and J.H. Green(1962), Structural control of interior drainage, southern San Joaquin Valley, California: U.S. Geol. Survey Prof. Paper 450-D, p.D89-91.

Dibblee, T.W., Jr. (1955), Geology of the southeastern margin of the San Joaquin Valley, California: in Earthquakes in Kern County, California during 1952, Calif. Div. Mines and Geology Bull. 171, p.23-24.

Dibblee, T.W., Jr. (1976), The Rinconada and related faults in the southern Coast Ranges, California, and their tectonic significance: U.S. Geol. Survey Prof. Paper 981, 55pp.

Dickinson, W.R., D.S. Cowan, and R.A. Scheickert (1972), Test of new global tectonics: discussion: Amer. Assoc. Petrol. Geol. Bull., v.56, p.375-384.

Fox, L.S. (1929), Structural features of the east side of the San Joaquin Valley, California: Amer. Assoc.

Geol. Bull., v.13, p.101-108.

Freund, R. (1974), Kinematics of transform and transcurrent faults: Tectonophysics, v. 21, p.93-134.

Garfunkel, Z. (1974), Model for the late Cenozoic tectonic history of the Mojave Desert, California, and for its relation to adjacent regions: Geol. Soc. America Bull., v.85, p.1931-1944.

Graham, S.A., and W.R. Dickinson (1978), Evidence for 115 kilometers of right slip on the San Gregorio-Hosgri fault trend: Science, v.199, p.179-181.

Hackel, O. (1966), Summary of the geology of the Great Valley: in Geology of Northern California, Calif. Div. Mines and Geology Bull. 190, p.217-238.

Hadley, D., and H. Kanamori (1977), Seismic structure of the Transverse Ranges, California: Geol. Soc. America Bull., v.88, p.1469-1478.

Hamilton, W., and W.B. Meyers (1966), Cenozoic tectonics of the western United States: Rev. Geophys., v.4, p.509-549.

Harding, T.P. (1976), Tectonic significance and hydrocarbon trapping consequences of sequential folding synchronous with San Andreas faulting, San Joaquin Valley, California: Amer. Assoc. Petrol. Geol., v.60, p.356-378.

Hay, E.A. (1976), Cenozoic uplifting of the Sierra Nevada in isostatic response to North America and Pacific plate interactions: Geology, v.4, p.763-766.

Heintz L.O., and J.W. Vernon (1965), Geology of south-central Tejon oil field (abstr.): Amer. Assoc. Petrol. Geol. Bull., v.49, p.1084-1085.

Henyey, T.L. (1976), Heat flow and tectonic patterns on the southern California borderland: in Aspects of the geologic history of the California continental borderland (Howell, D.G., ed.), Pacific Sec. Amer. Assoc. Petrol. Geol. Misc. Publ. 24, p.427-448.

Hill. D.P. (1982), Contemporary block tectonics, California and Nevada: Jour. Geophys. Research, v.87, p.5433-5450.

Hill, M.L., and T.W. Dibblee, Jr. (1953), San Andreas, Garlock, and Big Pine faults, California: Seismol. Soc. America Bull., v.64, p.443-458.

Hoots, H.W., T.L. Bear, and W.D. Kleinpell (1954), Geological summary of the San Joaquin Valley, California: in Geology of Southern California, Calif. Div. Mines and Geology Bull. 170, p.113-129.

Howell, D.G. (1975), Hypothesis suggesting 700 km of right slip in California along northwest-oriented faults: Geology, v.3, p.81-83.

Huffman, O.F. (1972), Lateral displacement of upper Miocene rocks and the Neogene history of offset along the San Andreas fault in central California: Geol. Soc. America Bull., v.83, p.2913-2946.

Jahns, R.H. (1973), Tectonic evolution of the Transverse Ranges province as related to the San Andreas Fault System: in Proc. Conference on Tectonic Problems of the San Andreas Fault System, Stanford Univ. Publ. Geol. Sci., v.13, p.149-170.

Johnson , J.D., and W.R. Normark, (1974), Neogene evolution of the Salinian block, west-central California: Geology, v.2, p.11-14.

Kammerling, M.J. and B.P. Luyendyk (1979), Tectonic rotations of the Santa Monica Mountains region, western Transverse Ranges, California, suggested by paleomagnetic vectors: Geol. Soc. America Bull., v.90, p.331-337.

Kanter, L.R., and M.O. McWilliams (1980), Tectonic rotation of the southernmost Sierra Nevada, California (abstr.): EOS (American Geophys. Union Transactions), v.61. p.948.

Karp, S.E. (ed.) (1968), Geology and oil fields, west side of the southern San Joaquin Valley: Amer. Assoc. Petrol. Geol.; Soc. Econ. Geol.; Soc. Econ. Paleontologists and mineralogists, 43rd Ann. Mtg. Guidebook, Amer. Assoc. Petrol. Geol. Pacific Sec., p.78-81.

Livaccari, R.F. (1979), Late Cenozoic tectonic evolution of the western United States: Geology, v.7, p.72-75.

Lofgren, B.E. (1965), Tectonic movement in the Grapevine area, Kern County, California: in Geol. Surv. Research, 1966, U.S. Geol. Survey Prof. Paper 550-B, p.B6-11.

Luyendyk, B.P., M.J. Kammerling, and R. Terres (1980), Geometric models for Neogene crustal rotations in southern California: Geol. Soc. America Bull., v.91, p.211-217.

MacPherson, B.A. (1978), Sedimentation and trapping mechanisms in Upper Miocene Stevens and older turbidite fans of southeastern San Joaquin Valley, California: Amer. Assoc. Petrol. Geol. Bull., v.62, p.2243-2274.

Moody, J.D. (1973), Petroleum exploration aspects of wrench-fault tectonics: Amer. Assoc. Petrol. Geol. Bull., v.57, p.449-476.

Moody, J.D., and M.J. Hill (1956), Wrench-fault tectonics: Geol. Soc. America Bull., v.67, p.1207-1246.

Nilsen, T.H., and T.W. Dibblee, Jr. (1974), Stratigraphy and sedimentology of the Cantua Sandstone Member of the Lodo Formation, Vallacitos area, California: in The Paleogene of the Panoche Creek-Cantua Creek area, central California, Soc. Econ. Paleontologists and Mineralogists Pacific Sec., Guidebook, p.36-68.

Nilsen, T.H., and S.H. Clarke, Jr. (1975), Sedimentation and tectonics in the early Tertiary continental borderland of central California: U.S. Geol. Survey Prof. Paper 925, 64pp.

Page, B. (1982), Sequential geologic indicators of plate interactions, Central California (abstr.): EOS, Amer. Geophys. Union Transactions, v.63, no.45, p.911.

Ross, D.C., C.M. Wentworth, E.M. McKee (1973), Cretaceous mafic conglomerates near Guala offset 350 mi. by San Andreas fault from ocean crustal source near Eagle Rest Peak, California: U.S. Geol. Surv. Jour. Research, v.1, p.45-52.

Savage, J.C., W.H. Prescott, M. Lisowski, N. King (1979), Strain in southern California: measured uniaxial north-south regional contraction: Science, v.202, p.883-885.

Scheidegger, A.E.(1959), Note on the tectonics of Kern County, California, as evidenced by the 1952 earthquakes: Jour. Geophys. Research, v.64, p.1499-1501.

Simonson, R.R. (1958), Oil in the San Joaquin Valley, California: in Habitat of Oil (Weeks, L.G., ed.), Amer. Assoc. Petrol. Geol., p.99-112.

Smith, G.I. (1962), Large lateral displacement on Garlock fault, California, as measured from offset dike swarm: Amer. Assoc. Petrol. Geol. Bull., v.46, p.85-104.

Smith, G.I., and J.P. Church (1980), Twentieth-century deformation in the Garlock fault-Slate Range area, southeastern California: Geol. Soc. America Bull., v.91, p.524-534.

Suppe, J. (1970), Offset of late Mesozoic basement terranes of the San Andreas fault system: Geol. Soc. America Bull., v.81, p.3253-3257.

Sylvester, A.G., and A.D. Darrow (1979), Structure and neotectonics of the western Santa Ynez fault system in southern California: Tectonophysics, v.52, p.389-405.

Taylor, J.G. (1976), Geologic appraisal of the petroleum potential of offshore southern California - the borderland compared to onshore coastal basins: U.S. Geol. Survey Circ. 730, 43pp.

Turner, D.L., G.H. Curtis, F.A.F. Berry, and R. Jack (1970), Age relationships between the Pinnacks and Parkfield felsites and felsite clasts in the southern Temblor Range, California - implications for San Andreas fault displacements (abstr.): Geol. Soc. America Abstr. with Programs, v.2, p.154.

Vail, P.R., and J. Hardenbol.(1979), Sea-level changes durin the Tertiary: in Ocean/continent boundaries, Oceanus, v.22, no.3, p.71-79.

Webb, G.W. (1981), Stevens and earlier Miocene turbidite sandstones, southern San Joaquin Valley, California: Amer. Assoc. Petrol. Geol. Bull., v.65, p.438-465.

Wilcox, R.E., T.P. Harding, and D.R. Seely (1973), Basin wrench tectonics: Amer. Assoc. Petrol. Geol. Bull., v.57, p.74-96.

Wright, L.A. (1976), Late Cenozoic fault patterns and stress fields in the Great Basin and westward displacement of the Sierra Nevada block: Geology, v.4, p.489-494.

Yeats, R.S. (1978), Neogene acceleration of subsidence rates in southern California: Geology, v.6, p.456-460.

Zieglar, D.L., and J.H. Spotts (1976), Reservoir and source bed history in the Great Valley of California: in Tomorrow's oil from today's provinces, Amer. Assoc. Petrol. Geol. Pacific Sec. Misc. Publ. 24, p.19-38.

Appendix I

"$^{40}Ar/^{39}Ar$ age spectrum analysis of detrital microclines from the southern San Joaquin Basin, California: An approach to determining the thermal evolution of sedimentary basins."

Foreword to Appendix I:

The rapid subsidence rate occurring in the southern San Joaquin Basin since the late Pliocene has important implications for the thermal evolution of this basin. Clearly, also, an understanding of the thermal history is relevant from an economic perspective since the southern San Joaquin Valley is one of the major on-land petroleum producing districts in the United States.

One way to test the thermal aspects of the basin is to experiment using detrital microcline separates from deep wells in the southern San Joaquin Basin's depocenter and analyze them by the $^{40}Ar/^{39}Ar$ age spectrum technique. Since partial loss of radiogenic argon from minerals through geological heating events follows fairly simple, well-known diffusion principles, it was felt that this technique might have considerable advantages over other temperature indicators which display apparent complexity over varying temperature conditions. Also, by using a technique which yields age information, it was hoped that chronologic constraints could be obtained on the thermal heating of the basin.

The paper which follows describes the initial application of the age spectrum technique to this problem.

Abstract

Detrital microcline grains from sedimentary strata preserve a record of thermal evolution in the temperature range ~100° to 200°C which can be revealed by $^{40}Ar/^{39}Ar$ age spectrum analysis. Microcline separates from deep drill hole intersections with Eocene to Miocenne sediments in the Basin and Tejon Blocks of the southern San Joaquin Valley, California, analysed by the the age spectrum approach show radiogenic ^{40}Ar ($^{40}Ar^*$) gradients that record both the slow cooling of the uplifting sediment source 65 Ma ago, and a recent thermal event. This information, in conjunction with the observation of fission track annealing in the coexisting apatites, allows estimation of the temperature-time conditions of this thermal event at about 140°C for ~200 ka. Present and paleotemperature data is in accord with heating related to several kilometers of Pleistocene sediment deposition. Heat flow calculations suggest that this recent subsidence has depressed the thermal gradient from about 30°C-km^{-1} to the present apparent gradient of 24°C-km^{-1}.

$^{40}Ar/^{39}Ar$ analysis of detrital microcline crystals yields thermochronological information in the temperature-time range of petroleum maturation and provides this technique with potential as both a useful exploration tool and as a means of probing the fundamental geodynamic processes of basin evolution.

1. Introduction

An understanding of the thermal evolution of sedimentary basins is important in a variety of geological disciplines for reasons related to the economic significance of these features, and because of implications for lithosphere tectonics and rheology. Recently, relatively simple thermal models (e.g., 1) have, with some variations, been successfully tested on a variety of active basins for which heat flow information is available (e.g., 2,3,). Understanding the mechanism of basin formation (e.g., extensional or compressional) allows temperature-time paths for the crust and lithosphere to be inferred. For the same approach to be successful in extant basins, however, requires techniques capable of yielding both paleotemperature and geochronological information.

An understanding of temperature and time are particularly important in assessing the economic potential of a sedimentary basin. Our knowledge of the inter-relationship between temperature and time in petroleum formation is only approximate because of the complexity of the process, but it has generally been observed that the rate of hydrocarbon generation from kerogen apparently doubles with every 10°C rise in temperature (4). Several studies have used this inference (5,6,7,) to predict the temperature-time trade-off within the zone of petroleum formation. For a short heating duration, a relatively high temperature

is required and vice versa. For a heating period on the order of $\sim 10^7$ years, these authors predict that significant petroleum generation will occur in the temperature interval between about 80°C and 150°C. Below this temperature range, the reaction kinetics are too sluggish to produce petroleum and above this range, "cracking" takes place which generates lower molecular weight species such as methane.

The importance of the knowledge of temperature in the analysis of sedimentary basins has led to the development of several methods of thermometry which include vitrinite reflectance, exinite and conodont color changes, carbon ratio theory, electron spin resonance and kerogen color changes (4, 8). The usefulness of these approaches to the understanding of the thermal evolution of a sedimentary pile is limited by the complexity of the thermally-activated reactions and this renders difficult the detailed theoretical understanding needed for precise temperature predictions. In addition, none of these techniques provides temporal information.

Recent research involving the $^{40}Ar/^{39}Ar$ age spectrum technique has indicated that this approach may have potential in this role. With the first application of the $^{40}Ar/^{39}Ar$ age spectrum technique to a variety of meteorites, Merrihue and Turner (9) and Turner et al. (10) demonstrated that both ages of crystallization and of reheating could be obtained from the data. A theoretical

model proposed by Turner (11) showed that these results could be interpreted as resulting from the diffusion loss of radiogenic ^{40}Ar ($^{40}Ar^*$) during a later thermal event. When lunar material became available, many excellent examples were shown supporting a model of radiogenic ^{40}Ar gradients due to partial outgassing (12). Recently, several studies of terrestrial samples have demonstrated the ability of amphiboles and K-feldspars to reveal diffusion gradients of $^{40}Ar^*$ imposed naturally as a result of a re-heating event or as result of slow cooling (13, 14, 15). This observation, in conjunction with known diffusion parameters, allows resolution of not only the age of the source and later heating event, but allows an estimate of the maximum temperature experienced during the events to be assessed. Calculations performed by Harrison and McDougall (15) indicated that microcline K-feldspar would be capable of preserving a record of thermal events in the temperature range of 100 to 200 C over geological time periods. We here report the results of an immediate application of this result - that of using detrital microclines in sedimentary basins to monitor the thermal evolution of the strata.

2. Experimental

High purity microcline/albite separates were obtained from drill core samples using heavy liquid and magnetic separation techniques. The separates were cleaned ultra-

sonically in 10% HF to remove surface contamination. In all cases, clean unaltered feldspars were recovered. With the exception of samples 9 and 11, ~65 mg of the greater than 0.150 mm diameter size fraction were wrapped in aluminum foil and sealed in an evacuated quartz amphoule for irradiation. Australian National University intralaboratory standard GA1550 biotite was included in the irradiation package. This mica has a K-Ar age of 97.9 Ma calculated using the decay constants and isotopic abundances recommended by Steiger and Jäger (16). Three flux monitors were placed at the center and both ends of the quartz amphoule to monitor a ~2 percent flux gradient. These samples were irradiated in the core of the Brookhaven National Laboratory High Flux Beam Reactor for a period of 3 hours, equivalent to a total fast neutron dose of $\sim 10^{18}$ neutrons-cm^{-2}. Factors used to correct the effects of interferring neutron reactions were $(^{40}Ar/^{39}Ar)_K = 1.25 \times 10^{-2}$, $(^{36}Ar/^{37}Ar)_{Ca} = 2.24 \times 10^{-4}$ and $(^{39}Ar/^{37}Ar)_{Ca} = 6.64 \times 10^{-4}$ (17).

The 0.150 mm diameter size fractions of samples 9 and 11 were irradiated for 30 hours in the core of the U.S. Geological Survey TRIGA reactor along with GA1550 biotite. A detailed description of irradiation techniques and correction factors used is given in Dalrymple et al. (18).

After loading the irradiated samples in the high vacuum extraction system, preheating at 200°C was accomplished to further remove any adsorbed atmospheric Ar.

Subsequent Ar extractions from the samples during stepwise-heating were carried out in a Mo crucible which was heated by means of a radiofrequency generator. With the exception of samples 9, 11, and 24 which were run at the U.S. Geological Survey Laboratory in Reston, Virginia, sample extractions and mass spectrometer analyses were carried out at SUNY at Stony Brook. For these samples, a thermocouple placed directly adjacent to the sample monitored the extraction temperatures. Uncertainty in these temperatures is about ± 30°C. Gas extractions were cleansed of active gases using a Ti getter heated to 800°C and a charcoal trap was used to remove any hydrocarbons present in the gas fractions. The isotopic composition of the Ar released from the samples was analyzed using a 20 cm radius, 60° magnetic sector-type rare gas mass spectrometer utilizing electron multiplier collection. High mass-36 blank values due to a residue of ^{36}Cl in the system limited precision in the small initial gas fractions. Samples 9, 11, and 24 were analyzed at the U.S. Geological Survey Laboratory, Reston, Virginia using a similar extraction system. The mass spectrometric analyses were carried out using Faraday cup collection on a Micromass 1200 instrument.

Uncertainties in the $^{40}Ar/^{39}Ar$ ages include the quadratically combined precision of the individual isotopic measurements of the samples and flux monitor, but the results from samples run at SUNY at Stony Brook tended to be dominated by a 13 percent uncertainty in the apparent ^{36}Ar

blank. At the editor's request, the data tables do not accompany this article, but can be obtained from the authors.

3. Geological and teconic setting

The San Joaquin Valley of central California has yielded in excess of 4 billion barrels of oil in this century (19) and as a result has been extensively studied by geologists (e.g., 20, 21, 22). The Tejon and Basin Blocks of the southern San Joaquin Valley have been the focus of a variety of geological and geochemical investigation including detailed stratigraphy (23,24, 25), organic geochemistry (26), zeolite thermometry (26,27), and fission track paleothermometry (28). On the basis of laumontite crystallization and fission track dating of detrital apatites., Briggs et al. (28) suggested that although both the Basin and Tejon Blocks had experienced a thermal event since the late Miocene, the Basin Block is presently at peak thermal conditions whereas the Tejon Block has cooled somewhat from a previously elevated temperature distribution. Because of ther well-documented nature, we chose to analyze detrital microcline grains from the drill cores used by Briggs et al. (28). These cores were obtained from Eocene to Miocene intersections of deep drill holes in the Tejon Oil Field area.

Figure 1 shows schematically the stratigraphy of the Basin and Tejon Blocks in the sampled area. The inset in Fig. 1 indicates the map location of the various deep

drill holes from which the cores were obtained. The sedimentary history of the area has been well-documented in several recent studies (e.g., 23,24, 25). Briefly, Eocene to Pliocene sandstones deposited in a marine environment have been further buried by Pleistocene to Holocene terrigenous sediments. Rocks of the Tejon Block appear to be at or near their maximum depth of burial, but have experienced elevated temperatures in the recent past (26). The Basin Block, sometimes referred to as the Maricopa sub-basin, contains several kilometers of recent, probably post-Pliocene sediment, and has been the prime depocenter since the late Miocene. Bounded on the south by the Tejon Block platform, the northern limit of the Maricopa sub-basin is the east-west trending Bakersfield arch. Clastic sediments in the basin have been derived from two major sources: the Sierra Nevada Range and more recently, the uplifted Tejon Block (24). Essentially all post-Pliocene sediment in the Tejon Block originated from the Tehachapi Range.

The Great Valley sequence developed in an oblique convergent margin setting in a subduction complex fore-arc basin as the Farallon plate was subducted eastwards under the North American plate (30). As subduction of the Farallon plate ridge initiated, a propagating dextral strike-slip boundary developed between the Pacific and North American plates starting at about 30 Ma ago (30, 31). The inception of the San Andreas fault system in southern California about 8-14 Ma ago (32) caused abrupt sediment-

ary discontinuities in the west as well as the formation of new major structures.

A schematic east-west cross-section of the present southern San Joaquin Valley can be viewed as a thick sequence of Upper Eocene to Recent sediments deposited on the shallowly west-dipping flank of the Sierra Nevada Range. In the west, the San Andreas system has disrupted the sequence with steeply-dipping right-lateral shear displacements. Although sedimentary strata generally dip inwards at the margins of the basin, they are tilted most severely along the western margin. Further, a tightly-folded and faulted northwest trending anticlinorium has evolved at various stratigraphic levels progressively eastwards from the immediate vicinity of the San Andreas fault (33). Although the thick sedimentary sequence appears to have accumulated more or less continuously as the basin subsided, several brief stages of uplift have occurred resulting in localized erosional unconformities in the stratigraphy (22). Oblique subduction of the Mendocino Fracture Zone late in the tectonic evolution of southern California has been proposed as a cause of uplift of the San Joaquin Basin (13-15 Ma ago (34). Still later uplifts have resulted from stresses developed in the Big Bend region of the San Andreas system. Earthquake epicenters along the White Wolf fault (35), because of uplift of the Tejon Block, indicate that these stresses continue to influence the region to the present.

4. Results and discussion

Results of $^{40}Ar/^{39}Ar$ age spectrum anlyses on eleven microcline separates from deep drill hole cores in the Tejon and Basin Blocks are shown in Figures 2 to 7. Although we anticipated observing a systematic decrease in K-Ar ages down the drill holes in a similar fashion to the variation in apatite fission track ages seen by Briggs et al. (28), the results (Table 1) give no clear indication of such a trend. Instead, the data scatter about an average age of 78 Ma which is somewhat younger than the average zircon fission track age of about 83 Ma measured from these cores by Briggs et al. (28). Indeed, because the deepest strata in the basin contains material presumably eroded from the higher levels of the uplifting, adjacent basement rocks, it is reasonable to suspect that prior to basin heating, detrital microcline ages might increase systematically with depth. This effect, coupled with later $^{40}Ar^*$ loss from samples deepest in the section, might obscure the expected younging trend.

These Cretaceous ages correspond to the time that the source of these sediments cooled sufficiently from high temperature during uplift to "close" with respect to $^{40}Ar^*$ loss and fission track erasure. The source to these sediments is likely to have been the adjacent Tehachapi and S erra Nevada Mountain Ranges. Several recent analyses of slowly cooling granitoid bodies have indicated that fission tracks cease to be erased from zircons at a temperature

of about 180°C, whereas microcline closes to $^{40}Ar^*$ loss at about 130°C (15, 36, 37). Thus the small contrast in age is likely to be the result of slow cooling in the temperature range 200° to 100°C between about 85 and 65 Ma. This is consistent with both the observation of ~65 Ma old apatite ages from high enough in the stratigraphic sequence to be removed from any post-Cretaceous thermal event (28) and the apparent absence of Cretaceous sediments in the basin.

Before continuing with the description of our age spectra, it is appropriate to consider the observation of Harrison and McDougall (15) who found that, as a result of slow cooling at a rate of $\lesssim 5°C\text{-}Ma^{-1}$, microclines from a large granitoid body contained $^{40}Ar^*$ loss gradients within their perthite lamellae. These profiles, when resolved using the $^{40}Ar/^{39}Ar$ age spectrum technique, corresponded to a spectrum of temperatures which Harrison and McDougall (15) assessed to be between 110°C to 180°C; approximately the closure temperatures of fission tracks in apatite and zircon, respectively. Thus, any structure in the age spectra of the thermally undisturbed detrital microclines in the basin will reflect the slow cooling of the source, which has imparted ages that rise from those indicated by the lower temperature gas fractions of ~65 Ma to terminal ages in the spectra at ~85 Ma. In fact, virtually all our analyses can be characterized by age gradients from about 65 Ma at zero percent ^{39}Ar released, to $\lesssim$80 Ma at the high temperature end of the age spectrum with variable

amounts of $^{40}Ar^{*}$ loss in recent times.

Samples 4 (Fig. 2), 1, 7 and 9 (Fig. 3), 10, 24 and 26 (Fig. 4) from the Tejon Block yield age spectra which are typified by sample 4, (Fig. 2) obtained from a depth of 3684 m. Apart from the initial gas fractions which correspond to very minor post-Oligocene loss (13) over the first 2 percent of the ^{39}Ar released, the age spectrum shows a virtual monotonic increase from an initial age at 61 Ma to 90 Ma in the last extraction step.

Our deepest sample from the Tejon Block, 26 (Fig. 4), has apparently experienced minor (~2 percent ^{40}Ar loss at some time since about 39 Ma - the youngest reliable age in the early gas release. Sample 24, however, (Fig. 4) although higher in the sequence (3557 m), has lost at least 5 percent $^{40}Ar^{*}$ during an event younger than about 37 Ma. This discrepancy is in part expected as laumontite thermometry of this sample indicates that the localized portion of the basin from which sample 24 was obtained has experienced post-alteration erosion and was originally deeper than other samples at a present comparable depth.

The relatively minor $^{40}Ar^{*}$ loss experienced by samples from the Tejon Block precludes our obtaining any significant thermochronological information from these samples. Samples 12 and 22 (Fig. 5), 14 (Fig. 6), and 11 (Fig. 7), however, from the Basin Block are substantially more interesting in providing clues to the thermal evolution of this portion of the San Joaquin Basin.

Samples 12 and 14 (Fig. 5 and 6), obtained from depths

of 3726 and 4435 m, respectively, show similar age spectra to those previously discussed with minor (~2%) $^{40}Ar^*$ loss superimposed on slow cooling gradients during the age range ~60 to 85 Ma. However, sample 22 (Fig. 5), taken from a depth of 6200 m shows significant $^{40}Ar^*$ loss. Compared to the virtually unaffected spectrum of sample 12, this sample appears to have lost about 18 percent $^{40}Ar^*$ during burial heating. Further, this loss has occurred since about 9 Ma, the youngest age obtained from the age spectrum This agrees with the conclusion of Briggs et al. (28) who, on the basis of stratigraphic, structural, and mineralogical evidence, concluded that the thermal event that has affected this areal occurred within the last 5 Ma. An extrapolation of this age spectrum to zero percent ^{39}Ar released is consistent with a contemporary thermal event. Definition of the age of heating from sample 22 is only approximate because of the relatively small amount of $^{40}Ar^*$ lost and the complication of determining near-zero K-Ar ages. For older basins, it should be possible to determine the age of heating by this approach to within several percent.

Because of poor resolution in the age spectrum of sample 11 (Fig. 7), about 630 m higher in the succession than 22, we are unable to determine the precise amount of $^{40}Ar^*$ lost, but can place a maximum limit of $\lesssim 8$ percent on this quantity. It seems likely that this sample has experienced at least several percent $^{40}Ar^*$ loss as it

yields the lowest K-Ar age of all samples measured from both tectonic blocks (Table 1).

Naeser et al. (27) have determined, on the basis of laumontite thermometry, that the Basin Block samples are currently at peak temperature conditions whereas the Tejon Block has cooled recently from previously elevated temperatures.

5. Thermal reconstruction

The observation of significant $^{40}Ar^*$ loss from sample 22 in recent times coupled with the conclusion of Naeser et al. (27) regarding the prograde condition of the Basin Block provides us with sufficient information to estimate the temperature-time history of this locality.

Diffusion loss of $^{40}Ar^*$

The loss of $^{40}Ar^*$ from microcline has previously been modeled by diffusion in an infinitely long and wide slab of finite thickness 2ℓ (15). The justification for this is that the plane sheet is a suitable description of the slab-like perthite lamellae whose incohernt boundaries control the effective diffusion half-width. Microscopic examination of our mineral separates reveal ubiquitous perthite and antiperthite development which leads us to adopt this model of $^{40}Ar^*$ diffusion in microcline.

The solution of Fick's Second Law for linear flow in a solid bounded by two parallel planes with initial and boundary conditions:

$C = C_o, \quad -\ell < x < +\ell, \quad t = 0$

$C = 0, \quad x = +\ell, \quad x = -\ell, \quad t > 0$ (1)

is given by (e.g., 38):

$$C_{x,t} = C_o \frac{4}{\pi} \sum_{n=o}^{\infty} \frac{(-1)^n}{2n+1} \exp\{-D(2n+1)^2\pi^2 t/4\ell^2\} \cos\frac{(2n+1)\pi x}{2\ell} \quad (2)$$

where $C_{x,t}$ is the concentration at distance x from the center of the slab after time t; D is the diffusion coefficient, and C_o is the initial, uniform concentration of $^{40}Ar^*$. This expression for a constant D is only valid for a square-pulse thermal history; and unlikely scenario for subsidence of a sedimentary basin. However, we can accomodate a time-dependent diffusion coefficient by c considering a geologically reasonable temperature history as consisting of a discrete number of isothermal steps. We can solve equation (2) numerically to yield the concentration distribution. The fraction of gas, f, remaining after time, t, is given by:

$$f = \frac{M_t}{M_\infty} = \frac{M_o - M_t}{M_o} = 1 - \sum_{n=o}^{\infty} \frac{8}{(2n+1)^2\pi^2} \exp\{-D(2n+1)^2\pi^2 t/4\ell^2\} \quad (3)$$

where $M_o = 2\ell C_o$; M_t is the mass of gas in solid at t; and M_∞ is the mass of gas in the solid after infinite time (i.e., zero concentration). For a fractional loss of less than 0.5, Jost (39) has formulated a convenient approximation to equation (3):

$$f \approx 2\pi^{-\frac{1}{2}} \left(\frac{Dt}{\ell^2}\right)^{\frac{1}{2}} \quad (4)$$

Substituting the well-known Arrhenius relationship, $D/\ell^2 = D_o/\ell^2 \exp(-E/RT)$, where D_o/ℓ^2 is the frequency/grain size parameter, E is the activation energy, R is the gas

constant, and T is the absolute temperature, we can rewrite equation (4) in terms of temperature:

$$T \approx -E/R \ln [(f/(2\pi^{-1/2}))^2 / (D_o/\ell^2 \cdot t)] \quad (5)$$

Thus to solve for the temperature experienced by our samples, we require knowledge of the diffusion parameters for $^{40}Ar^*$ in microcline (i.e., E and D_o/ℓ^2) and an estimate of the time scale of heating. Harrison and McDougall (15) calculated values of D/ℓ^2 from the measured ^{39}Ar release from microcline samples during stepwise gas extractions. When plotted against the reciprocal absolute temperature of the extraction step, the data below about 900°C define an activation energy of 29 ±2 kcal-mol^{-1} and a D_o/ℓ^2 of 6^{+14}_{-4} sec^{-1}. The large uncertainty in the latter parameter reflects imprecise temperature monitoring. This activation energy agrees fairly well with previous estimates of 24, 26, and 32 kcal-mol^{-1} (40,41,42, respectively), but contrasts sharply with extimates of E from homogeneous K-feldspars of between 40 to 52 kcal-mol^{-1} (15). Although our uncertain sample temperature control during extraction (see section 2) precludes us from deriving an accurate diffusion law for our samples, for illustration we point out that the eight $\lesssim$800°C gas fractions from sample 22 yield a moderately well-correlated Arrhenius relationship (r=0.93) and corresponds to an E = 27 kcal-mol^{-1} and D_o/ℓ^2 = 5, remarkably (but probably fortuitously) similar to the values of Harrison and McDougall (15). However, this gives us some confidence in adopting E = 30 kcal-mol^{-1} and D_o/ℓ^2 =

6 sec^{-1} for our calculations.

The second question regarding the time scale of heating can be addressed with reference to the study of apatite fission track age variations in the deep drill-holes from the Basin Block of Briggs et al. (28). The kinetics of fission track annealing have been extensively studied in recent years (e.g., 43, 44, 45, 46, 47, 48) by both laboratory annealing and geological experiments. A synthesis of both these approaches allowed Gleadow and Duddy (46) to constrain the temperature-time requirements for apatite fission track fading (Fig. 8). This diagram represents the temperature-time conditions necessary to induce both 50 percent and total fission track fading in apatite. For the moment we shall return to the apatite fission track age study of Briggs et al. (28). As was previously mentioned, detrital apatites in the Basin Block have experienced variable annealing during a recent, possibly active, thermal event. The ages drop to half of their original value of ~60 Ma at a presently measured temperature of about 130°C. On the basis of laumontite thermometry which indicates a paleotemperature equivalent to the contemporary temperature (28), we can return to Fig. 8 and deduce a heating period from this temperature of approximately 200 ka. With our estimates of E, D_o/ℓ^2 and t, we calculate a temperature from equation (5) for sample 22 of 160°C, which corresponds well with the presently measured temperature of 6200 m at 157°C (27). These calculations imply an isothermal temperature history: that is, a sudden rise to the

present temperature approximately 200,000 years ago. A more likely thermal history over perhaps the past million years is of a slowly increasing temperature resulting from the post-Pliocene sediment accumulation and consequent burial of the sequence including sample 22.

Thermal calculations

We can obtain the functional form of a heating history, T(z,t), for samples accumulating in a compressional basin where subsidence of the basin is matched by deposition, by solution of the heat conduction equation in a semi-infinite moving medium. The equation:

$$\frac{\partial^2 T}{\partial z^2} - \frac{U}{\kappa}\frac{\partial T}{\partial z} - \frac{1}{\kappa}\frac{\partial T}{\partial t} = 0 \qquad (6)$$

solved together with boundary and initial conditions:

$$T(0,t) = T_s$$
$$T(z,0) = T_s + (Gz) \qquad (7)$$

yields the expression (e.g., 49):

$$T(z,t) = T_s + (Gz) + (GUt) + (G/2)\{(z-Ut)\exp(-Uz/\kappa) \times \operatorname{erfc}[(z-Ut)/2(\kappa t)^{1/2}] - (z+Ut)\operatorname{erfc}[(z+Ut)/2(\kappa t)^{1/2}] \qquad (8)$$

where T is temperature at the sample depth below the earth's surface, z; t is the time since onset of subsidence at velocity U; G is the geothermal flux; and is the thermal diffusivity.

Our interest is to determine what likely combination of geothermal gradient and subsidence rate was responsible for creating a temperature-time history sufficient to induce 18 percent $^{40}Ar^*$ loss in microcline. We have evaluat-

ed equation (8) for a variety of possible post-Pliocene histories. The present measured temperature of 6200 m of 157°C (Table 1) corresponds to an apparent geothermal gradient of about 24°C-km^{-1}, assuming a surface temperature of 10°C. If no post-Pliocene sediment had been deposited in the Basin Block (i.e., U=0), then this would represent the equilibrium gradient. However, weveral kilometers of post-Pliocene sediment have accumulated in this area - the exact amount is uncertain because of the lack of key fossils in this non-marine environment. Assuming a constant rate of deposition over the last 2 Ma, we can estimate both the Pliocene geothermal gradient and rate of subsidence of the basin.

Using a reasonable value of $K = 10^{-6}$ m^2-sec^{-1}, we have evaluated equation (8) for a variety of values of U and G. The results of these calcualtions are summarized in Fig. 9. This diagram represents the present temperature at 6200 m resulting from vari combinations of subsidence rate and the initial Pliocene thermal gradient. The amount of accumulated sediment resulting from different average subsidence rates over the past 2 Ma is shown on the right vertical axis.

Clearly, for sample 22 to have reached 157°C given even modest (1 to 2 km) Quaternary sediment deposition, requires that the thermal gradient have been about 30°C-km^{-1} (Fig.9). We should point out that we have in fact made two assumptions regarding the post-Pliocene basin history. The first has been explicitly stated, that the

Quaternary sediments have accumulated at a constant rate. If, however, several kilometers of fill had been deposited in the basin shortly after the Pliocene-Pleistocene boundary and none subsequently, our estimate of the Pliocene thermal gradient would be too high as considerable time would have elapsed to allow the 157°C isotherm to relax back to its predeposition depth. Our second assumption is implicit in equation (6), that of heat conduction in a moving medium. If convective overturn of ground water has occurred to significant depths in the Quaternary, then it is possible that rapid subsidence would not suppress the isotherms because of rapid transport of heat by this mechanism. Indeed, it is possible to obtain an apparent gradient at 6200 m that is in excess of the equilibrium thermal gradient. However, the relatively uniform apparent gradient of $24^{\circ}C\text{-}km^{-1}$ deep in the drill holes (27,28) suggests that such forced upward transport of heat is presently not occurring, giving us some confidence in the general validity of our model.

Having arrived at our conclusion regarding the necessity of a somewhat elevated Pliocene heat flux to accomodate at least a kilometer of Quaternary sediment deposition, we have computed the possible temperature history of sample 22 over the past 2 Ma using the preferred values of G and U. Results of these calculations show a virtually linear increase of temperature with time. We have divided this temperature history into 10^5 year increments (Δt) and evaluated the fractional loss of $^{40}Ar^*$ from microcline

using equation (4) that would result from exposure to the average temperature over that increment for a time, Δt. Since negligible loss has occurred from sample 14 at a present temperature of 120°C, we begin our accumulation at the time corresponding to this temperature. For example, the first 10^5 years at an average temperature of 124°C would cause about 2.5 percent ^{40}Ar loss, whereas the fifth increment, at a temperature of 140°C would generate about 5 percent loss. Our quota of 18 percent loss would be realized by the time the temperature rose to 145°C. This value is reasonably close to the present measured down-hole temperature of 157°C. In fact, by relatively small adjustment of the activation energy (~5 percent) we could match the observed loss to the thermal history exactly.

6. Summary and conclusions

We have described an approach to reconstructing the thermal history of a sedimentary basin which utilizes the ability of the $^{40}Ar/^{39}Ar$ age spectrum technique to resolve the intra-crystalline distribution of $^{40}Ar^*$ in K-feldspars. In the case of a basin formed in a compressional environment, this approach can yield information on both the age and the maximum temperature experienced by a sample as a result of heating associated with burial. Although our analysis is somewhat speculative, we have illustrated the ability of this thermochronological information to help constrain estimates of depositional

rate and of pre-subsidence geothermal flux. This approach would be usefully applied to microcline samples from basins which have formed durin lithospheric extension to obtain thermal information related to both the initial rifting and subsequent heating during burial. Geologists have need to understand the thermal history of sedimentary rocks, as petroleum maturation from kerogens occurs in a relatively narrow temperature window- probably about 90° to 150°C over the periods of time appropriate to basin formation. We have demonstrated in this paper that detrital microcline feldspars can yield thermochronological information over this temperature range which provides this technique with potential both as a useful exploration tool for the petroleum industry and as a means of probing the fundamental geodynamic processes of basin evolution.

References

1. D. McKenzie, Some remarks on the development of sedimentary basins, Earth Planet. Sci. Lett. 40 (1978) 25-32.
2. S.J. Hellinger and J.G. Sclater, Some comments on two-layer extensional models for the evolution of sedimentary basins, in press, Jour. Geophys. Res. (1983).
3. L. Royden, F. Horvath, A. Nagmarosy and L. Stegena, Evolution of the Pannonian Basin System: Part II, Subsidence and Thermal history, in press, Tectonics (1983).
4. J. M. Hunt, Petroleum geochemistry and geology. (freeman, San Francisco, 1979) 617pp.
5. J. Connan, Time-temperature relation in oil genesis, AAPG Bull 58 (1974) 2516-2521.
6. N. V. Lopatin, The determination of the influence of temperature and geologic time on the catagenic process of coalification and oil-gas formation, in: Research on organic matter of modern and fossil deposits (in Russian). Moscow. Acad. Nauk. USSR, (1976) 361-366.
7. D. W. Waples, Time and temperature in petroleum formation: Application of Lopatin's method to petroleum exploration, AAPG Bull. 64 (1980) 916-926.
8. B. P. Tissot and D. H. Welte, Petroleum Formation and Occurrence, (Springer—Verlag, Berlin, 1978) 538pp.
9. G. Merrihue and G. Turner, Potassium-argon dating by activation with fast neutrons, Jour. Geophys. Res. 71

(1966) 2853-2857.

10. G. Turner, J. A. Miller and R. L. Grasty, The thermal history of the Bruderheim meteorite, Earth Planet. Sci. Lett. 1 (1966) 155-157.

11. G. Turner, The distribution of potassium and argon in chondrites, in Origin and distribution of the elements (ed. L. H. Ahrens, Pergamon) (1968) 387-398.

12. G. Turner, Argon 40 - Argon 39 dating of lunar rock samples. Proc. 1st Lunar Sci. Conf. 2 (1970) 1665-1684.

13. T. M. Harrison and I. McDougall, Investigations of an intrusive contact, northwest Nelson, N. Z. - II: Diffusion of radiogenic and excess ^{40}Ar in hornblende revealed by $^{40}Ar/^{39}Ar$ age spectrum analysis, Geochim. Cosmochim. Acta 44 (1980) 2005-2020.

14. T. M. Harrison, Diffusion of ^{40}Ar in hornblende, Contrib. Mineral. Petrol. 78 (1981) 324-331.

15. T.M. Harrison and I. McDougall, The thermal significance of potassium feldspar K-Ar ages inferred from $^{40}Ar/^{39}Ar$ age spectrum results, Geochim. Cosmochim. Acta 46 (1982) 1811-1820.

16. R. H. Steiger and E. Jäger, Subcommission on geochronology: convention on the use of decay constants in geo- and cosmochronology, Earth Planet. Sci. Lett. 36 (1977) 359-362.

17. R. Warasila, unpublished data.

18. G. B. Dalrymple, E. C. Alexander, M. A. Lanphere and G. P. Kraker, Irradiation of samples for $^{40}Ar/^{39}Ar$

dating using the Geological Survey TRIGA reactor, Geol. Surv. Prof. Paper 1176 (1981) 55pp.

19. D. L. Zieglar and J. H. Spotts, Reservoir and source bed history in the Great Valley of California, in: Tommorrow's Oil from Today's Provinces, AAPG Pac. Sec. Misc. Pub. 24 (1976) 19-38.

20. H. W. Hoots, T. L. Bear, and W. D. Kleinpell, Geological summary of the San Joaquin Valley, California, R. H. Jahns, ed., Calif. Div. Mines Bull. 170 (1954) 113-129.

21. R. R. Simonson, Oil in the San Joaquin Valley, California, in: Habitat of Oil, L. G. Weeks, ed., AAPG (1958) 99-112.

22. D. C. Callaway, Petroeum potential of San Joaquin Basin, California, in: Future Petroleum Provinces of the United States, I. M. Cram, ed., AAPG (1971) 239-253.

23. O. L. Bandy and R. E. Arnal, Middle Tertiary basin development, San Joaquin Valley, California, Geol. Soc. America Bull. 80 (1969) 783-819.

24. B. A. MacPherson, Sedimentation and trapping mechanism in Upper Miocene Stevens and older turbidite fans of southeastern San Joaquin Valley, California, AAPG Bull. 62 (1978) 2243-2274.

25. G. W. Webb, Stevens and earlier Miocene turbidite sandstones, southern San Joaquin Valley, California, AAPG Bull. 65 (1981) 438-465.

26. J. R. Castaño and D. M. Sparks, Interpretation of vitrinite reflectance measurements in sedimentary rocks and determination of burial history using vitrinite reflectance and authigenic minerals, Geol. Soc. America Spec. Paper 153 (1974) 31-52.

27. N. D. Naeser, C. W. Naeser and T. H. McCulloh (1982) Manuscript in preparation.

28. N. D. Briggs, C. W. Naeser and T. H. McCulloh, Thermal history of sedimentary basins by fission track dating, Nucl. Tracks 5 (1981) 235-237.

29 W. R. Dickinson, Plate tectonics and the continental margin of California, in: The Geotectonic Development of California (W. G. Ernst, ed., Prentice-Hall, Englewood Cliffs, N. J., 1981) 1-28.

30. T. Atwater, Implications of plate tectonics for the Cenozoic tectonic evolution of western North America, Geol. Soc. America Bull. 81 (1970) 3513-3536.

31 T. Atwater and P. Molnar, Relative motion of the Pacific and North American plates deduced from the sea-floor spreading in the Atlantic, Indian, and South Pacific oceans, in: Proc. Conf. on Tectonic Problems in the San Andreas Fualt System, R. L. Kovach and A. Nur, eds., Stanford Univ. Pubs. Geol. Sci. 13 (1973) 136-148.

32. J. C. Crowell, Problems concerning the San Andreas fault system in Southern California, Stanford Univ. Pubs. Geol. Sci. 13 (1973) 125-135.

33. T. P. Harding, Tectonic significance and hydrocarbon trapping consequences of sequential folding synchronous with San Andreas faulting, San Joaquin Valley, California, AAPG Bull. 60 (1976) 356-378.

34. D. P. Loomis and A. F. Glazner, Effect of Farallon Plate subduction on Miocene evolution of the San Joaquin basin, California, Geol. Soc. America Abstr. with Programs 14 (1982) 549.

35. H. Benioff, Mechanism and strain characteristics of the White Wolf fault as indicated by the aftershock sequence, Calif. Div. Mines Bull. 171 (1955) 199-202.

36. T. M. Harrison and I. McDougall, Investigations of an intrusive contact, northwest Nelson, N.Z. - I: Thermal, chronological and isotopic constraints on the region, Geochim. Cosmochim. Acta 44 (1980) 1985-2004.

37. T. M. Harrison, R.L. Armstrong, C. W. Naeser and J. E. Harakal, Geochronology and thermal history of the Coast Plutonic Complex, near Prince Rupert, B. C., Canadian Jour. Earth Sci. 16 (1979) 400-410.

38. J. Crank, Mathematics of diffusion (Oxford Univ. Press, Oxford, 1975) 2nd ed., 414pp.

39. W. Jost, Diffusion in Solids, Liquids and Gases (Academic Press, New York, New York, 1960) 558pp.

40. J. F. Evernden, G. H. Curtis, R. W. Kistler and J. Obradovich Argon diffusion in glauconite, microcline, sanidine, leucite and phlogopite, Am. J. Sci. 258 (1960) 583-604.

41. A. W. Laughlin, Excess radiogenic argon in pegmatite minerals. Ph. D. thesis, University of Arizona (1969) 187pp.

42. E. K. Gerling, L. K. Levskiy and J. M. Morazova, On the diffusion of radiogenic argon from minerals, Geochem. 6 (1963) 551-564.

43. C. W. Naeser and H. Faul, Fission track annealing in apatite and sphene, Jour. Geophys. Res. 74 (1969) 605-710.

44. C. W. Naeser, Fission track dating and geologic annealing of fission tracks, in: Lectures in Isotope Geology, E. Jäger and J. C. Hunziker, eds. (Springer-Verlag, Berlin, 1979) 154-169.

45. C. W. Naeser, The fading of fission tracks in the geologic environment - data from deep drill holes, Nucl. Tracks 5 (1981) 248-250.

46. A. J. W. Gleadow and I. R. Duddy, A natural long-term annealing experiment for apatite, Nucl. Tracks 5 (1981) 169-174.

47. Burchart, J. Galazka-Friedman and J. Kral, Experimental artifacts in fission-track annealing curves, Nucl. Tracks 5 (1981) 113-120.

48. R. A. Zimmerman and A. M. Gaines, A new approach to the study of fission track fading, U.S. Geological Survey Open-File Report 78-701 (1978) 467-468.

Figure captions

Fig. 1. Sample location map (insert) and structural profile of the southern San Joaquin Basin, from (27). The profile shows the three wells from which the samples were obtained. The Pliocene to Holocene designations represent conventional thought but may be poorly constrained.

Fig. 2. $^{40}Ar/^{39}Ar$ age spectrum analysis of a microcline separate obtained from 3.7 km depth in the Tejon Block. This spectrum is typical of the seven microclines analyzed from this region which show very minor $^{40}Ar^{*}$ loss in recent time superimposed on an age gradient which corresponds to slow cooling in the temperature range 200° to 100°C between about 85 to 60 Ma ago.

Fig. 3 $^{40}Ar/^{39}Ar$ age spectrum results for samples 1, 7, and 9 from depths between 2.2 and 2.9 km in the Tejon Block. These analyses show little indication of recent heating but preserve a gradient in age imposed during slow cooling of the sediment source terrane.

Fig. 4. $^{40}Ar/^{39}Ar$ age spectrum analyses of Tejon Block samples 10, 24, and 26 obtained from depths of 3.3, 3.6 and 4.4 km, respectively. Sample 24 appears to have lost considerably more $^{40}Ar^{*}$ than expected for its present depth, but evidence obtained from laumontite thermometry (27) indicates that this sample has been at a considerably

higher temperature than other samples currently at a comparable depth.

Fig. 5. $^{40}Ar/^{39}Ar$ age spectrum analyses of microclines from Basin Block samples 12 and 22. Sample 12, from a depth of 3.7 km, has experienced virtually no $^{40}Ar^*$ loss in the course of erosion from the adjacent Sierra Nevada Range and subsequent burial in the San Joaquin Basin. Sample 22, obtained at a depth of 6.2 km, exhibits 18 percent $^{40}Ar^*$ loss because of a recent thermal event.

Fig. 6. $^{40}Ar/^{39}Ar$ age spectrum analysis of microcline separated from Basin Block sample 14, taken from a depth of 4.44 km. This spectrum has remained undisturbed since the time of uplift in the sediment source region.

Fig. 7 $^{40}Ar/^{39}Ar$ age spectrum analysis of a microcline separate from Basin Block sample 11. The poor resolution in the early portion of gas release precludes our obtaining any detailed thermochronological information from this sample beyond estimating the maximum $^{40}Ar^*$ loss to be ≤ 8 percent.

Fig. 8. Arrhenius-type plot for fission track fading in apatite showing drill hole data of Gleadow and Duddy (46) for 0, 50, and 100 percent track loss (solid blocks), experimental annealing results of Naeser and Faul (circles), and the drill hole data of Naeser (44) for totally annealed apatites (crosses). A 50 percent track loss at a tempera-

ture of 130 C implies a heating period on the order of about 200 ka.

Fig. 9. Results of a thermal analysis of the subsidence-related heating of sample 22 displayed in terms of the rate of deposition versus the pre-subsidence geothermal gradient. Sample 22, currently at a depth of 6.2 km and a temperature of 157 C, has experienced about 1 and 3 km of burial since the Pliocene (Fig. 1). Assuming a constant deposition rate, the temperature of 6.2 km for a variety of subsidence rates and Pliocene thermal gradients are shown by the curved isotherms. The stippled area denotes a region of probable sediment accumulation in the Quaternary as well as the temperature range recently experienced by sample 22. These restrictions imply that the pre-Pleistocene thermal gradient in the area was 30 C-km^{-1}.

Table 1. Sample depth, temperature and microcline K-Ar age data.

Sample[1] Number	Depth[1] (m)	Present temperature[1] (°C)	Paleo-temperature[2] (°C)	K-Ar age[3] (Ma)
Tejon Block				
1	2195	75	97	76.3
7	2838	94	121	78.5
9	2907	95	123	76.9
10	3306	104	126	85.8
24	3557	106	146	72.9
4	3684	107	141	81.6
26	4398	115	152	80.7
Basin Block				
12	3726	104	96	76.2
14	4435	102	114	82.4
11	5572	144	144	72.2
22	6200	157	157	73.2

[1]Sample locations and temperatures from [27].
[2]Based on laumontite thermometry [27, 28].
[3]Incremental total fusion ages.

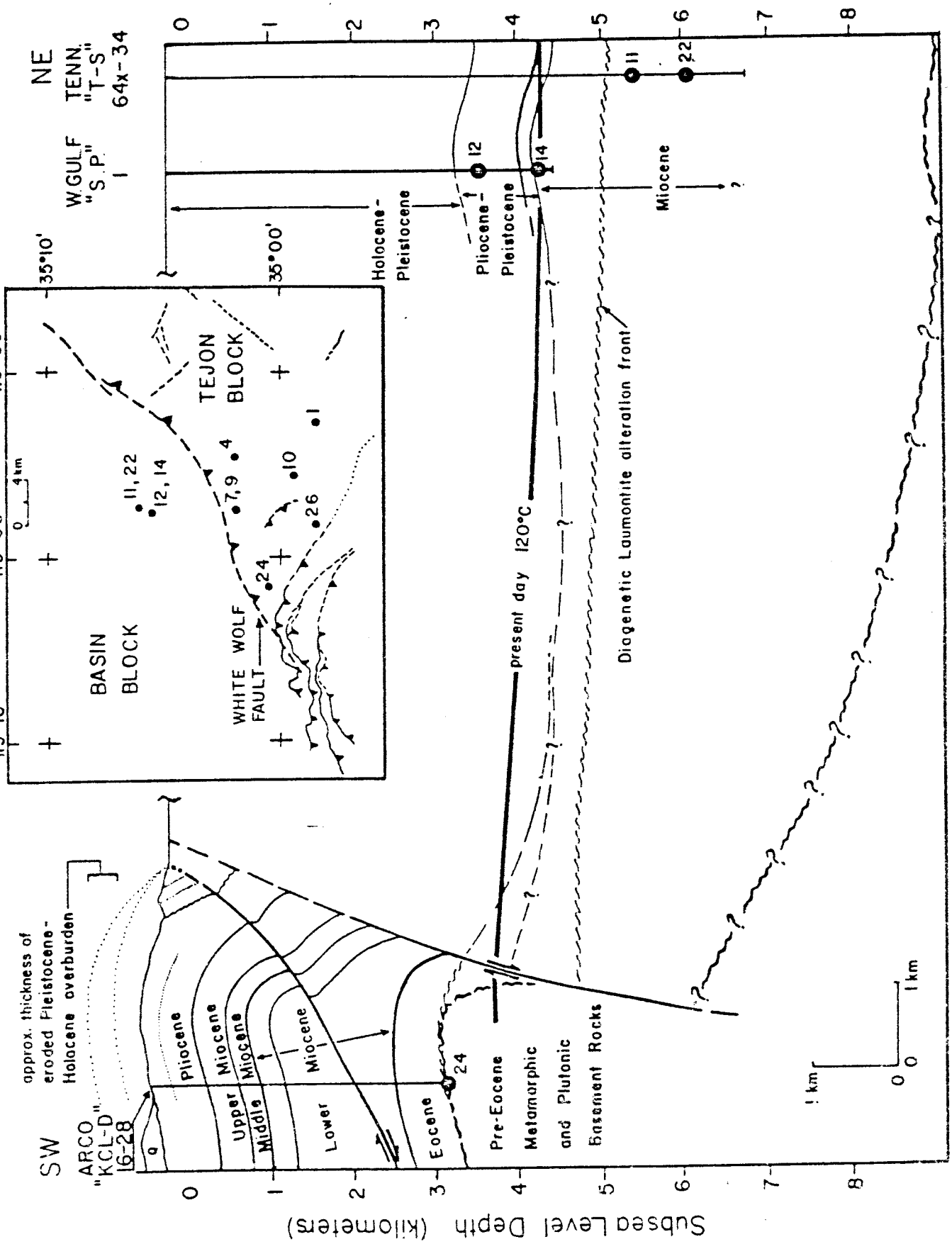
SW
ARCO "KCL-D" 16-28
approx. thickness of eroded Pleistocene - Holocene overburden
Pliocene
Miocene
Upper
Middle
Lower
Miocene
Miocene
Eocene
24
Pre-Eocene Metamorphic and Plutonic Basement Rocks
present day 120°C
Diagenetic Laumontite alteration front
NE
W.GULF "S.P." 1
TENN. "T-S" 64x-34
11
22
12
14
Holocene-Pleistocene
Pliocene-Pleistocene
Miocene
35°10'
35°00'
119°10'
119°00'
118°50'
BASIN BLOCK
TEJON BLOCK
WHITE WOLF FAULT
11, 22
12, 14
7, 9
4
10
26
24
1
4 km
1 km
Subsea Level Depth (kilometers)

Figure 1

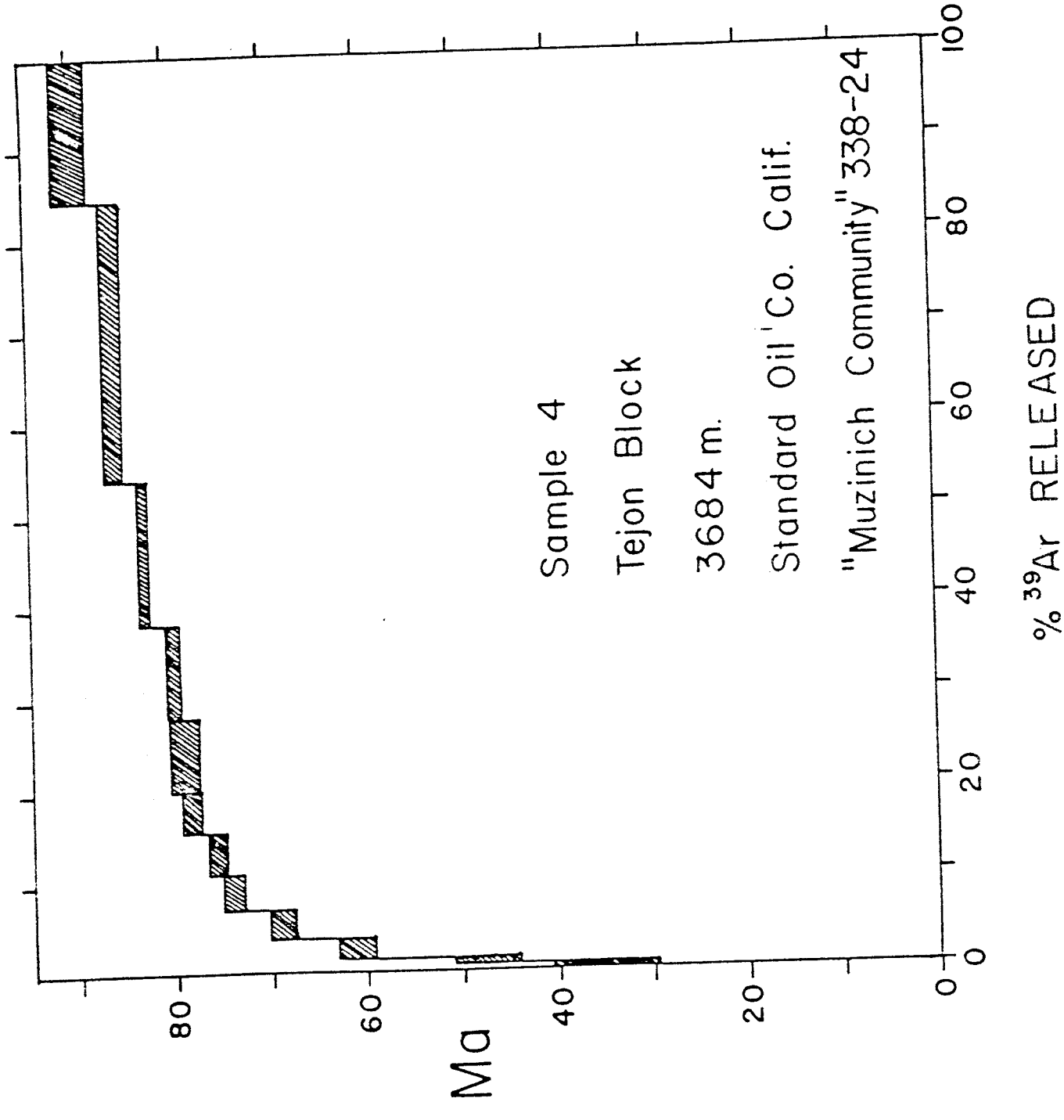
Sample 4
Tejon Block
3684 m.
Standard Oil Co. Calif.
"Muzinich Community" 338-24
Ma
80
60
40
20
0
0
20
40
60
80
100
% 39Ar RELEASED

Figure 2

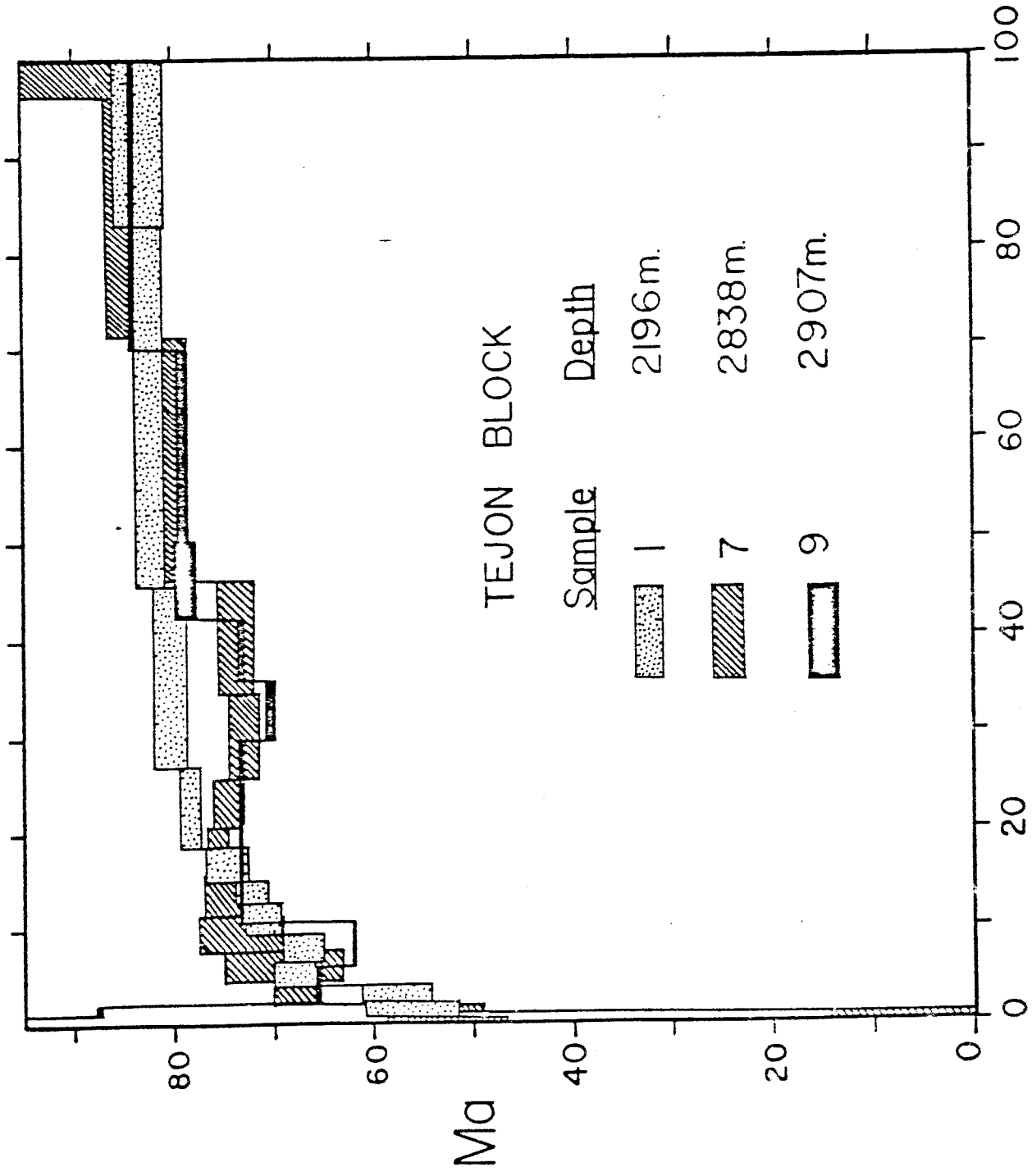
TEJON BLOCK
Sample Depth
1 2196m.
7 2838m.
9 2907m.
Ma
0
20
40
60
80
0
20
40
60
80
100
% ^{39}Ar RELEASED

Figure 3

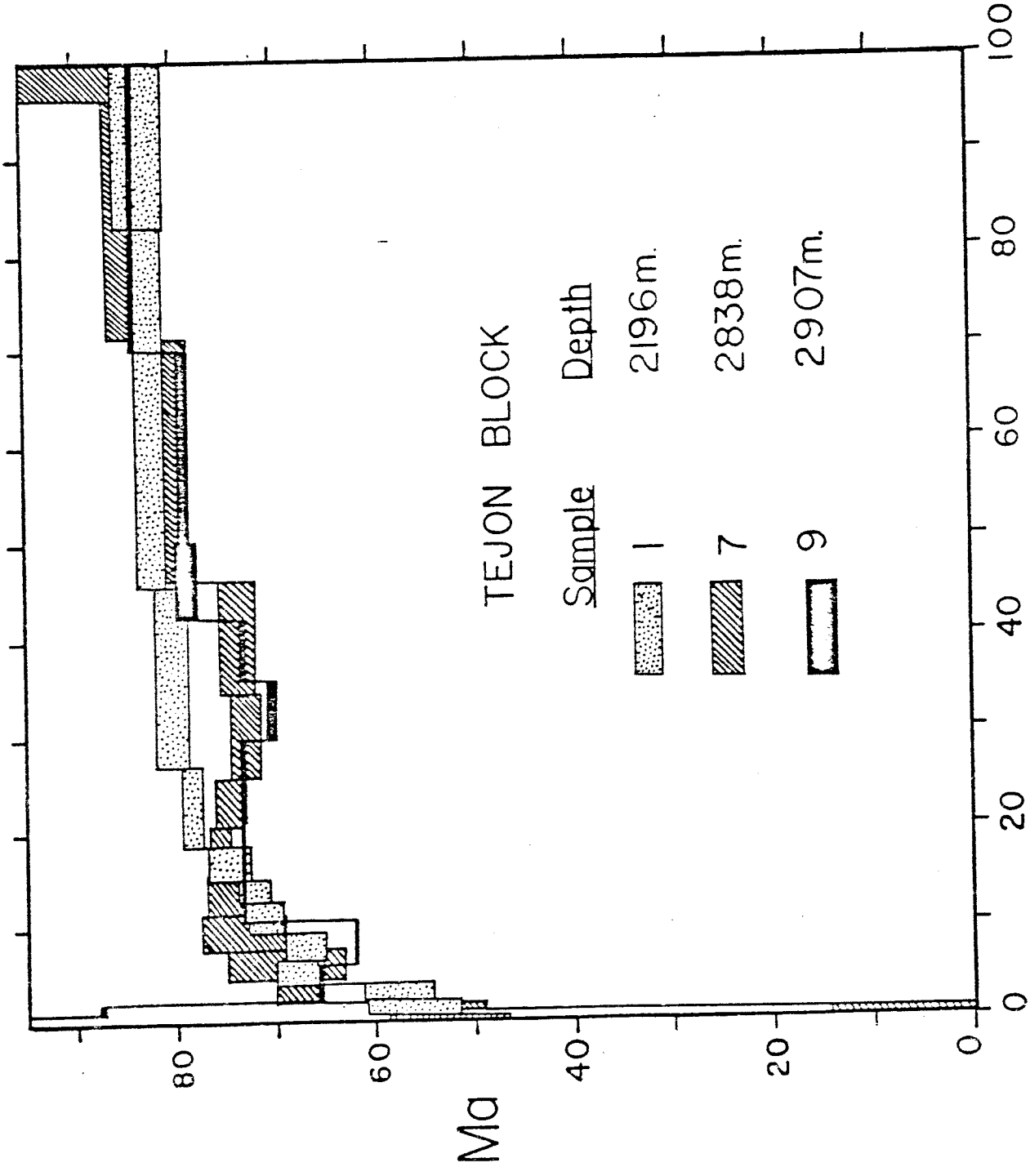
TEJON BLOCK
Sample Depth
1 2196m.
7 2838m.
9 2907m.
Ma
0
20
40
60
80
0
20
40
60
80
100
% ^{39}Ar RELEASED

Figure 4

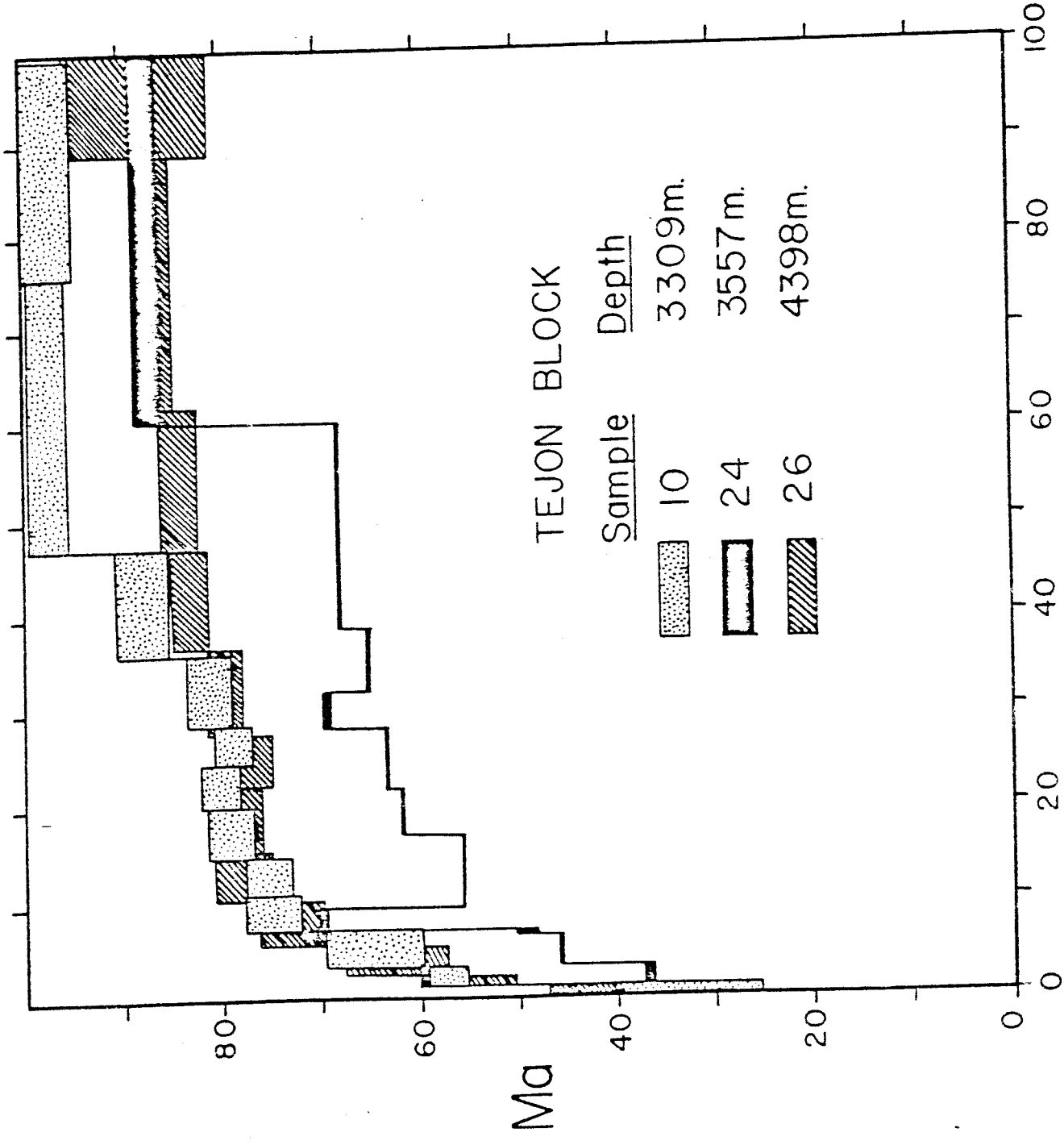
TEJON BLOCK
Sample
Depth
10
3309m.
24
3557m.
26
4398m.
Ma
0
20
40
60
80
0
20
40
60
80
100
% ^{39}Ar RELEASED

Figure 5

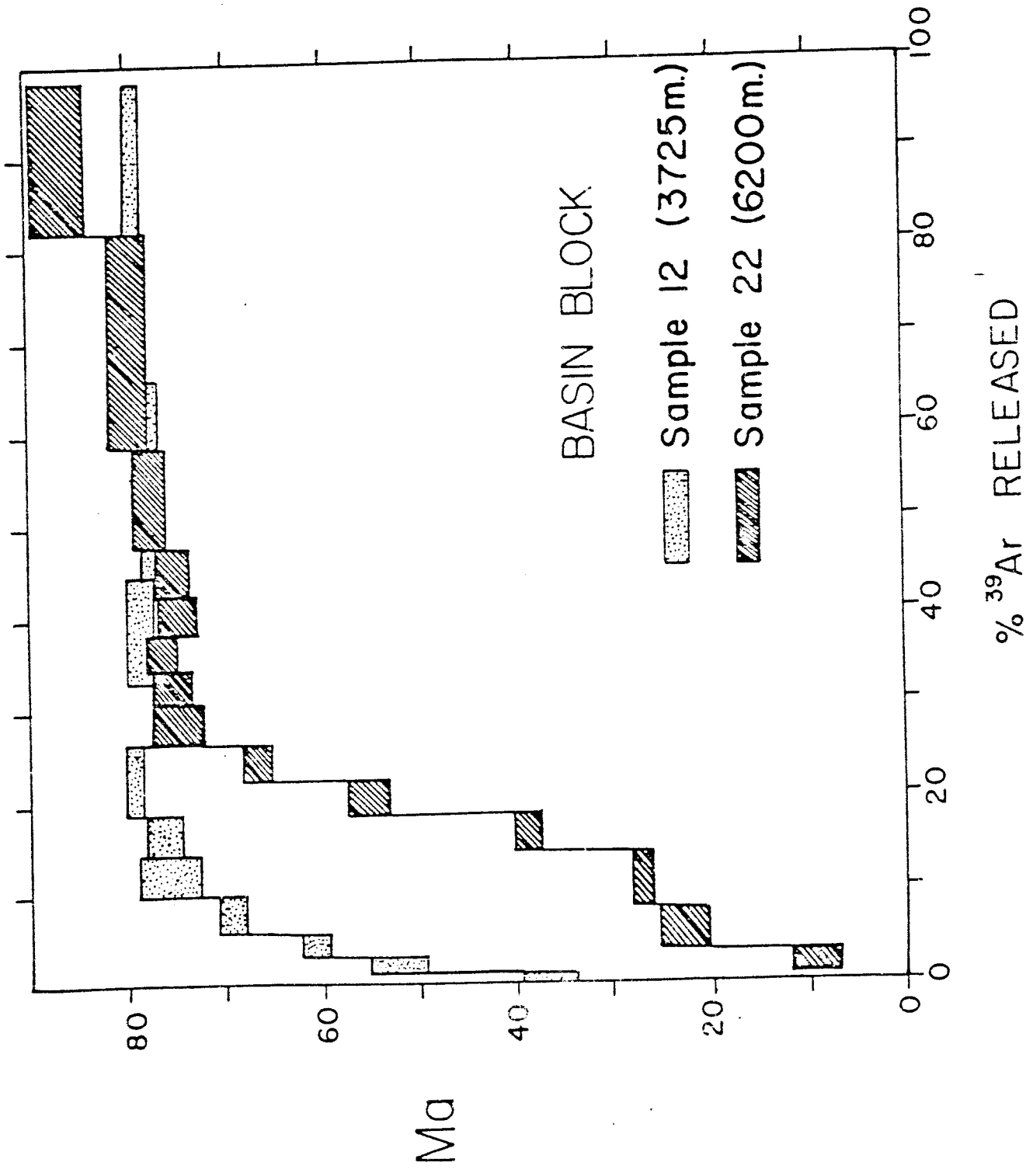
BASIN BLOCK
Sample 12 (3725m.)
Sample 22 (6200m.)
Ma
80
60
40
20
0
0
20
40
60
80
100
% ^{39}Ar RELEASED

Figure 6

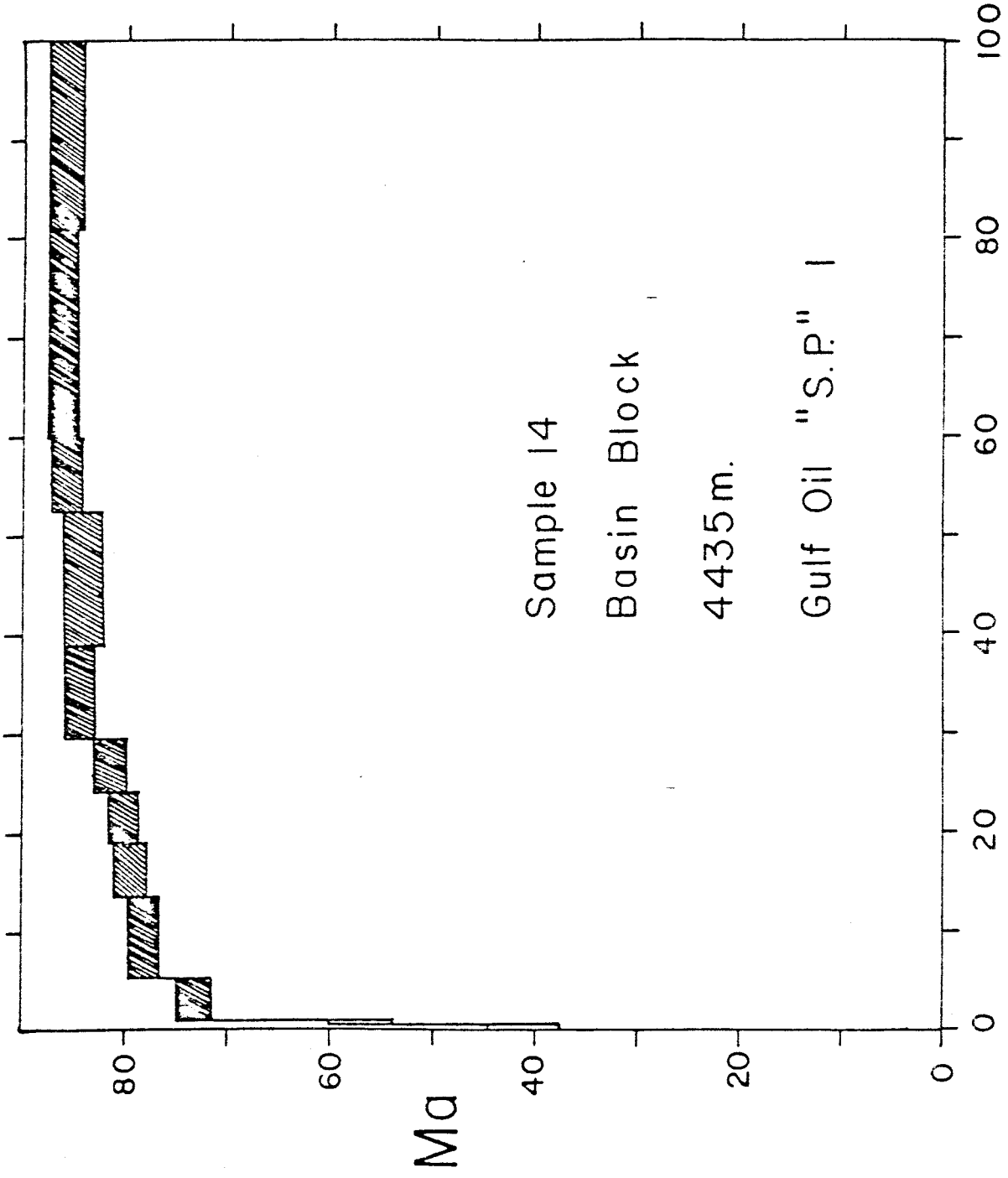
Sample 14
Basin Block
4435m.
Gulf Oil "S.P." 1
Ma
0
20
40
60
80
0
20
40
60
80
100
% ^{39}Ar RELEASED

Figure 7

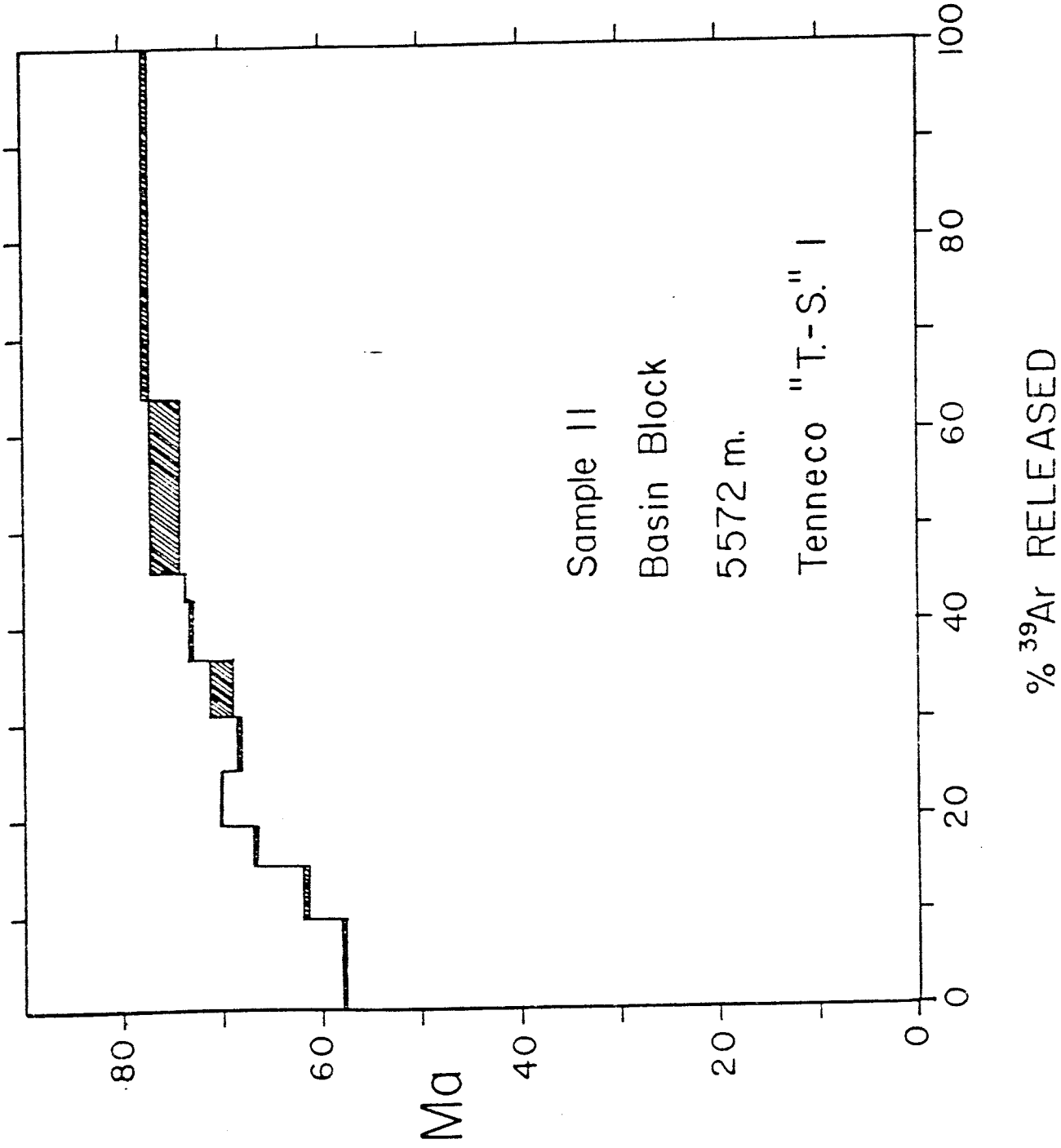
Sample 11
Basin Block
5572 m.
Tenneco "T.-S." 1
Ma
0
20
40
60
80
0
20
40
60
80
100
% 39Ar RELEASED

Figure 8

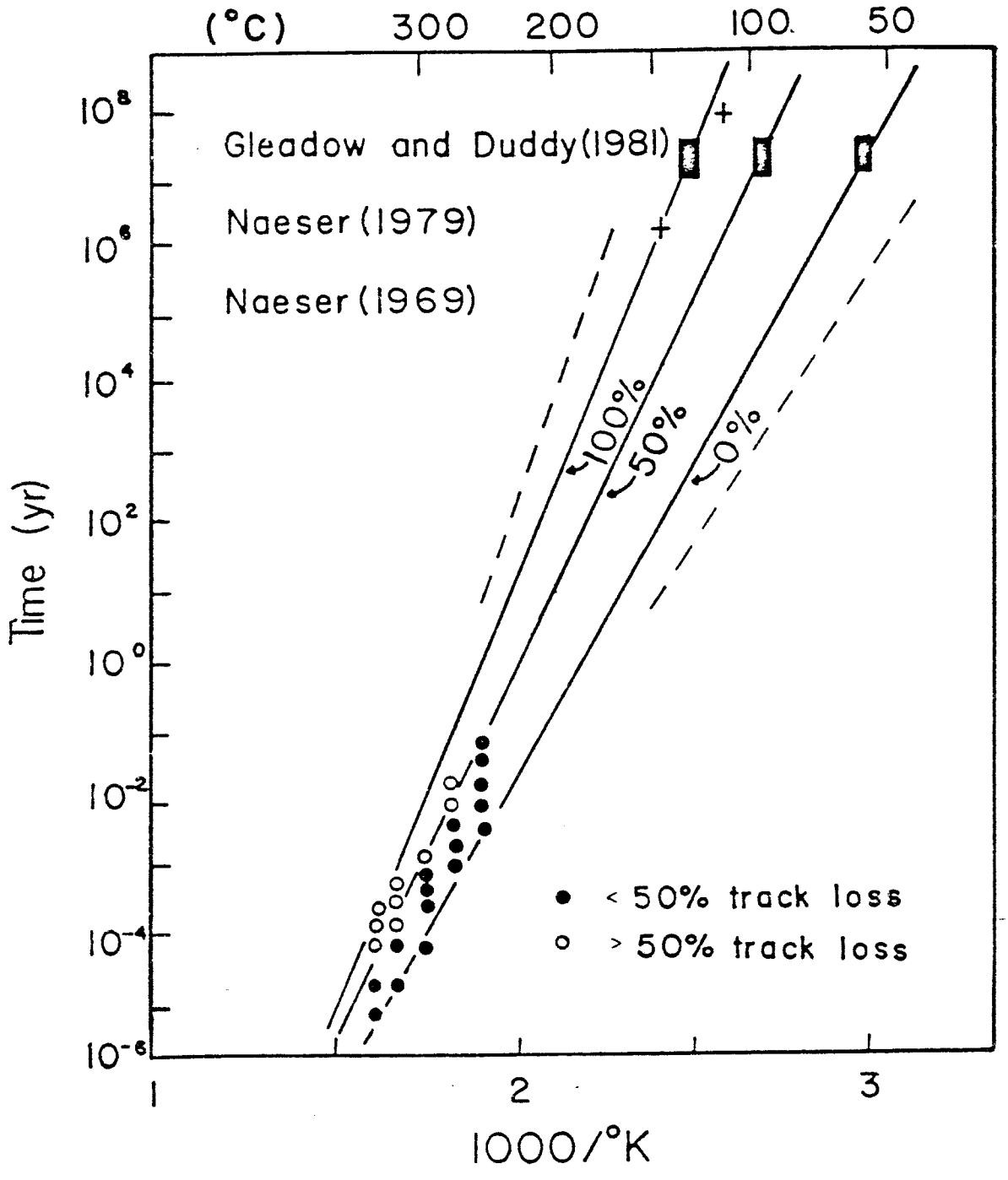
(°C)
300
200
100
50
Gleadow and Duddy(1981)
Naeser(1979)
Naeser(1969)
100%
50%
0%
< 50% track loss
> 50% track loss
Time (yr)
1000/°K

Figure 9

Quaternary Sediment Thickness (km)
6
4
2
200°C
160°C
130°C
110°C
90°C
40
30
20
Pliocene Thermal Gradient (°C-km⁻¹)
3
2
1
Subsidence Rate (mm-a⁻¹)

Figure 10

Appendix II

Tabulated data for the $^{40}Ar/^{39}Ar$ incremental heating runs of microcline separates from the Tejon and Basin Blocks.

Table 1(a) $^{40}Ar/^{39}Ar$ age spectrum results of microcline separates from the Tejon Block

Step Temperature (^0C)	$^{40}Ar/^{39}Ar$[1]	$^{37}Ar/^{39}Ar$[2]	$^{36}Ar/^{39}Ar$[1] ($\times 10^{-4}$)	$^{39}Ar_K$[3] ($\times 10^{-12}$ moles)	Cumulative ^{39}Ar (%)	Radiogenic ^{40}Ar (%)	$^{40}Ar^*/^{39}Ar_K$	Apparent Age[5] ± 1 s.d. (Ma)
1 (0.0673 g)	J=0.01407[4]							
400	30.35	0.00	1142.86	0.0066	0.026	0.0	0.000	--
450	4.66	0.00	119.68	0.0168	0.091	24.1	1.125	28.3± 27.9
500	2.30	0.00	38.09	0.0528	0.30	50.9	1.166	29.3± 28.9
500	2.31	0.00	6.79	0.148	0.87	91.3	2.106	52.7± 6.2
600	2.45	0.00	6.15	0.409	2.45	92.6	2.262	56.5± 4.8
650	2.95	0.00	21.37	0.400	4.0	78.5	2.312	57.7± 3.4
700	3.34	0.00	20.69	0.705	6.7	81.7	2.730	68.0± 2.0
750	3.21	0.00	17.37	0.724	9.5	84.0	2.693	67.1± 1.9
800	3.25	0.00	13.55	0.742	12.4	87.7	2.851	70.9± 1.8
850	3.27	0.00	12.56	0.761	15.4	88.7	2.901	72.2± 1.8
900	3.32	0.00	10.87	0.879	18.8	90.3	2.998	74.5± 1.9
1000	3.45	0.00	10.03	2.157	27.1	91.4	3.155	78.3± 1.0
1000	3.52	0.00	10.00	4.780	45.6	91.6	3.227	80.1± 1.5
1200	3.55	0.00	8.11	9.735	83.3	93.3	3.312	82.1± 1.3
1350	3.64	0.00	9.67	4.316	100.0	90.5	3.355	83.2± 2.4
								76.3

4 (0.0708 g) J=0.01407 [4]

400	66.72	0.00	2659.57	0.0053	.016	0.0	0.000	--
450	5.24	0.00	150.90	.0241	.091	14.6	0.763	19.3± 12.6
500	1.91	0.00	16.74	.124	.48	73.9	1.402	35.5± 5.6
550	2.12	0.00	6.89	.378	1.65	90.3	1.902	47.6± 3.4
600	2.59	0.00	4.36	.717	3.9	95.0	2.442	60.9± 2.1
650	2.86	0.00	3.04	1.028	7.1	96.8	2.757	68.6± 1.3
700	3.07	0.00	2.92	1.248	10.9	97.2	2.967	73.8± 1.0
750	3.15	0.00	3.06	1.530	15.7	97.1	3.040	75.5± 0.9
800	3.23	0.00	2.12	1.475	20.2	98.1	3.149	78.2± 1.0
900	3.25	0.00	2.07	2.518	28.0	98.1	3.174	78.8± 1.3
1000	3.30	0.00	2.36	3.310	38.3	97.9	3.213	79.7± 0.7
1100	3.43	0.00	2.85	4.928	53.5	97.5	3.332	82.6± 0.6
1200	3.56	0.00	3.33	9.831	84.0	97.2	3.446	85.4± 1.0
1350	3.68	0.00	0.50	5.169	100.0	99.6	3.642	90.1± 2.2
								81.6

7 (0.0648 g) J=0.01407 [4]

425	55.99	0.00	2267.60	0.0048	0.013	0.0	--	--
450	3.12	0.00	95.37	0.043	0.13	9.2	0.285	7.2± 7.2
500	1.57	0.00	0.00	0.130	0.48	100.0	1.543	38.7± 5.0
550	2.23	0.00	2.52	0.407	1.6	96.5	2.060	51.5± 2.7
600	2.78	0.00	1.60	0.963	4.2	98.3	2.716	67.6± 2.0
650	3.01	0.00	7.56	1.019	7.0	92.5	2.772	69.0± 5.8
700	3.15	0.00	6.62	1.475	11.0	93.8	2.935	73.0± 4.9
750	3.08	0.00	1.89	1.632	15.4	98.2	3.006	74.7± 1.7
800	3.11	0.00	2.34	1.756	20.1	97.8	3.020	75.0± 1.0
850	3.08	0.00	2.68	1.728	24.8	97.4	2.982	74.1± 1.6
950	2.97	0.00	1.73	3.258	33.6	98.3	2.902	72.2± 1.5
1050	3.01	0.00	1.90	4.328	45.4	98.1	2.743	73.2± 2.0
1150	3.23	0.00	0.50	7.531	65.8	99.5	3.201	79.5± 1.7
1250	3.48	0.00	1.59	10.955	95.5	98.6	3.421	84.8± 1.4
1375	3.79	0.00	4.60	1.677	100.0	96.4	3.642	90.1± 5.1
								78.5

9 (0.4738 g) J=0.00415[4]

13.501	0.0241	361.20	0.338	0.74	20.9	2.822	21.0±	0.3
76.529	0.0473	2212.00	0.074	0.9	14.6	11.173	81.7±	9.2
46.485	0.0624	867.30	0.049	1.0	44.9	20.872	149.8±	5.8
15.568	0.0213	121.50	0.0456	2.0	76.9	11.972	87.5±	0.5
10.057	0.0148	38.79	1.82	6.0	88.6	8.911	65.5±	0.4
8.854	0.0139	15.21	2.05	10.5	94.9	8.402	61.8±	0.3
10.336	0.0129	11.50	4.34	20.0	96.7	9.995	73.3±	0.4
10.301	0.0139	10.64	4.40	29.7	96.9	9.982	73.2±	0.4
10.118	0.0139	18.02	2.62	35.4	94.7	9.582	70.3±	0.5
10.857	0.0090	30.19	3.03	42.0	91.7	9.956	73.1±	0.4
11.740	0.0126	33.19	3.58	50.0	91.6	10.754	78.8±	2.0
11.947	0.0087	37.74	9.22	70.1	90.0	10.752	79.1	0.6
12.732	0.0072	40.74	13.60	100.0	90.5	11.522	84.3	0.4
							76:9	

10 (0.0648 g) J=0.01383[4]

300	767.57	0.00	38462.00	0.0004	0.002	0.0	--	--
350	61.96	0.00	5555.60	0.0012	0.007	0.0	--	--
400	19.12	0.00	1004.00	0.004	0.025	0.0	--	--
450	3.54	0.00	136.65	0.032	0.17	0.0	--	--
500	1.99	0.00	23.22	0.169	0.93	65.9	1.324	32.7 7.5
550	2.30	0.00	0.00	0.501	3.2	100.0	2.324	57.1 2.0
600	2.82	0.00	7.48	0.853	7.0	92.3	2.632	64.5 5.2
650	3.11	0.00	2.85	0.862	10.8	97.3	3.061	74.8 2.8
700	3.24	0.00	7.04	0.836	14.6	93.7	3.070	75.0 2.3
750	3.25	0.00	1.92	1.278	20.3	98.3	3.233	78.9 2.7
800	3.23	0.00	0.00	0.982	24.7	100.0	3.273	79.9 2.0
850	3.26	0.00	2.32	0.846	28.5	97.9	3.228	78.7 2.2
950	3.35	0.00	2.54	1.738	36.2	97.8	3.314	80.8 2.3
1050	3.62	0.00	3.31	2.518	47.5	97.3	3.568	86.9 2.7
1150	4.07	0.00	5.25	6.351	75.9	96.2	3.966	96.3 1.9
1250	4.05	0.00	5.43	5.148	98.9	96.1	3.947	95.9 2.4
1350	4.95	0.00	21.40	0.252	100.0	87.4	4.392	106.4 21.3
								85.8

24 (0.2680 g) J=0.01396 [4]

90.672	0.2942	2946.00	0.11	0.6	4.0	3.627	89.5	16.4
12.383	0.0785	368.80	0.46	3.0	12.0	0.178	37.0	0.5
6.487	0.0639	157.10	0.67	6.5	28.4	1.842	45.9	0.4
6.100	0.0597	138.80	0.16	7.3	32.8	2.001	49.6	1.2
8.476	0.0669	190.50	0.42	9.5	33.6	2.848	70.3	0.7
4.234	0.0800	66.92	1.42	16.9	53.3	2.257	56.0	0.3
3.803	0.1031	43.90	0.89	21.6	65.9	2.506	62.1	0.5
3.898	0.1359	45.07	1.32	28.5	66.0	2.573	63.6	0.4
4.214	0.1542	47.52	0.71	32.2	66.8	2.815	69.6	0.7
4.652	0.1085	67.97	1.26	38.8	56.9	2.647	65.4	0.4
5.362	0.0846	88.17	4.15	60.4	51.4	2.756	68.1	0.4
10.111	0.0911	221.10	7.60	100.0	35.4	3.579	87.9	1.3
							72.9	

26 (0.685 g) J=0.01360 [4]

400	154.69	0.00	3246.80	0.0028	0.012	38.0	58.857	1061.0	814.0
425	6.99	0.00	596.66	0.0037	0.038	0.0	--	--	
450	3.03	0.00	64.74	0.015	0.11	36.8	1.116	27.2	27.7
475	2.25	0.00	28.38	0.035	0.26	62.7	1.412	34.3	24.9
500	2.24	0.00	20.73	0.072	0.58	72.7	1.629	39.5	8.2
550	2.66	0.00	12.16	0.328	2.0	86.5	2.305	55.7	4.9
600	3.11	0.00	17.08	0.788	5.5	83.8	2.609	62.9	5.3
650	3.33	0.00	9.13	0.982	9.8	91.9	3.058	73.5	3.3
700	3.51	0.00	9.03	1.268	15.4	92.4	3.239	77.8	2.9
750	3.42	0.00	5.37	1.483	21.9	95.3	3.256	78.2	2.1
800	3.41	0.00	6.39	1.324	27.7	94.5	3.225	77.5	2.2
900	3.42	0.00	3.48	2.004	36.6	97.0	3.319	79.7	1.8
1000	3.56	0.00	3.37	2.368	47.0	97.2	3.465	83.1	1.7
1100	3.70	0.00	5.72	3.481	62.3	95.4	3.531	84.6	1.8
1200	3.72	0.00	3.80	5.897	88.2	97.0	3.613	86.6	1.6
1350	3.72	0.00	1.11	2.670	100.0	99.1	3.689	88.3	4.0
								80.7	

Table 1(b) $^{40}Ar/^{39}Ar$ age spectrum results of microcline separates from the Basin Block

Step Temperature (^0C)	$^{40}Ar/^{39}Ar$	$^{37}Ar/^{39}Ar$	$^{36}Ar/^{39}Ar$ (x 10^{-4})	$^{39}Ar_K$ (x 10^{-12} moles)	Cumulative ^{39}Ar (%)	Radiogenic ^{40}Ar (%)	$^{40}Ar^*/^{39}Ar_K$	Apparent Age ± 1 s.d. (Ma)	
11 (0.4676 g) J=0.00426 [4]									
	13.522	0.2342	199.80	2.45	9.4	56.4	7.626	57.7	0.3
	10.776	0.0508	89.25	1.44	14.9	75.5	8.136	61.5	0.4
	11.078	0.0217	75.63	0.61	17.2	79.8	8.840	66.7	0.4
	11.400	0.00	86.12	0.52	19.2	77.6	8.846	66.8	0.5
	10.800	0.0160	50.28	1.49	24.9	86.2	9.310	70.2	0.4
	10.117	0.0845	35.33	1.43	30.4	89.6	9.065	68.4	0.5
	10.403	0.0144	36.81	1.56	36.4	89.5	9.311	70.2	1.2
	10.955	0.0136	41.75	1.61	42.6	88.7	9.717	73.2	0.5
	12.555	0.0113	94.83	1.18	47.1	77.6	9.743	73.4	0.4
	12.783	0.0863	92.42	4.35	63.7	78.6	10.047	75.7	1.7
	14.00	0.0137	125.0	9.50	100.0	73.6	10.304	77.5	0.6
								72.2	

12 (0.0695 g) J=0.01383 [4]

350	1196.18	0.00	50000.00	0.0006	0.001	0.0	--	--	
450	33.71	0.00	981.35	0.017	0.046	14.2	4.799	115.9	113.0
500	3.96	0.00	134.61	0.071	0.23	0.0	--	--	
550	2.49	0.00	35.55	0.339	1.1	57.8	1.439	35.5	2.8
600	2.82	0.00	23.58	0.851	3.2	75.3	2.124	52.2	3.1
650	3.17	0.00	24.03	1.293	6.5	77.6	2.460	60.4	1.5
700	3.26	0.00	15.11	1.260	9.7	86.3	2.816	68.9	1.5
750	3.23	0.00	4.38	1.715	14.1	96.0	3.098	75.7	3.2
800	3.22	0.00	3.93	1.658	18.3	96.4	3.106	75.9	1.7
900	3.31	0.00	2.15	3.033	26.0	98.1	3.243	79.1	0.8
1000	3.24	0.00	4.05	2.848	33.3	96.3	3.120	76.2	0.7
1100	3.29	0.00	2.94	4.094	43.7	97.4	3.199	78.1	1.0
1200	3.31	0.00	4.14	8.726	65.8	96.3	3.183	77.7	0.6
1300	3.31	0.00	1.56	12.821	98.4	98.6	3.260	79.5	0.7
1400	3.40	0.00	19.37	0.621	100.0	83.2	2.829	69.2	12.9
								76.2	

14 (0.0653 g) J=0.01383 [4]

300	17.95	0.00	223.46	0.0042	0.012	63.7	11.585	268.1	251.0
400	11.66	0.00	729.93	0.0078	0.033	0.0	--		
450	1.30	0.00	63.64	0.037	0.13	28.9	0.766	19.0	11.0
500	2.22	0.00	19.55	0.121	0.46	74.2	1.662	41.0	3.6
550	2.69	0.00	13.15	0.288	1.2	85.7	2.327	57.1	3.2
600	3.09	0.00	4.36	1.521	5.4	95.9	2.995	73.2	1.7
650	3.29	0.00	4.10	3.005	13.5	96.4	3.204	78.2	1.4
700	3.40	0.00	5.64	2.013	19.0	95.1	3.263	79.6	1.7
750	3.39	0.00	4.52	1.886	24.1	96.1	3.288	80.2	1.6
800	3.42	0.00	3.62	1.960	29.4	96.9	3.343	81.5	1.7
900	3.45	0.00	0.55	3.465	38.9	99.5	3.467	84.5	1.4
1000	3.48	0.00	2.21	3.207	47.6	98.1	3.453	84.2	1.9
1100	3.55	0.00	1.87	4.652	59.9	98.5	3.533	86.1	1.5
1200	3.55	0.00	1.53	8.051	81.8	98.7	3.544	86.3	1.3
1350	3.56	0.00	2.05	6.699	100.0	98.3	3.540	86.2	1.6
								82.4	

22 (0.0678 g) J=0.01360[4]

400	41.62	0.00	795.54	0.0182	0.30	43.5	18.108	397.2	364.1
500	2.25	0.00	63.11	0.174	3.2	17.1	0.383	9.4	2.6
550	1.55	0.00	20.60	0.291	8.0	60.7	0.938	22.9	2.6
600	1.86	0.00	24.37	0.349	13.7	61.2	1.137	27.7	1.1
650	2.87	0.00	43.03	0.279	18.3	55.8	1.603	38.9	1.5
700	2.56	0.33	8.67	0.213	21.8	90.0	2.301	55.6	2.1
750	2.80	0.68	1.12	0.262	26.1	98.8	2.770	66.7	1.6
800	3.10	0.98	1.06	0.277	30.6	99.0	3.068	73.8	1.6
835	3.18	1.06	1.52	0.194	33.8	98.6	3.132	75.3	2.3
885	3.22	0.83	1.21	0.243	37.8	98.9	3.183	76.5	1.7
935	3.16	0.69	1.21	0.243	41.8	98.9	3.124	75.1	1.8
985	3.16	0.32	0.88	0.335	47.3	99.2	3.134	75.3	1.4
1085	3.31	0.29	2.40	0.653	58.1	97.9	3.241	77.8	1.5
1185	4.23	0.32	30.55	1.422	81.5	78.7	3.331	79.9	2.0
1285	5.42	0.56	59.71	1.017	98.2	67.4	3.653	87.5	3.4
1385	8.47	0.84	2.70	0.109	100.0	98.1	8.390	195.0	70.4
								73.2	

Footnotes.

[1] Corrected for blank .
[2] Corrected ^{37}Ar decay.
[3] Estimated from mass spectrometer sensitivity.
[4] Flux monitor used GA1550 biotite = 97.9 Ma(K/Ca = 38.5).
[5] Calculated using $\lambda = 5.543 \times 10^{-10}$ a^{-1}.

Appendix III

Additional samples analyzed by the $^{40}Ar/^{39}Ar$ dating technique

Appendix 3

Two samples in addition to those obtained from the San Joaquin Basin were separated and analyzed by the $^{40}Ar/^{39}Ar$ dating technique. These included a pegmatitic microcline from the Himalaya Mine, California, and a sample of microcline from a depth of 6.3 km in the Los Angeles Basin.

Both samples were reported to have undergone geological heating sufficient to be recorded in laumontite thermometry (McCulloh, T., personnal communication, 1982). The age spectra plots, however, indicate that virtually no loss disturbance has affected the argon profiles for the two samples. Clearly, either the temperature reached or the time duration of heating was insufficient to cause outgassing.

The Himalaya Mine microcline yielded a "flat age spectra" or plateau indicating an original cooling age of about 94 Ma. No monotonic rise from slow cooling is evident.

Sample 21 from the Los Angeles Basin, on the other hand, does show a well-developed slow cooling gradient rising to a maximum recorded age of about 83 Ma old.

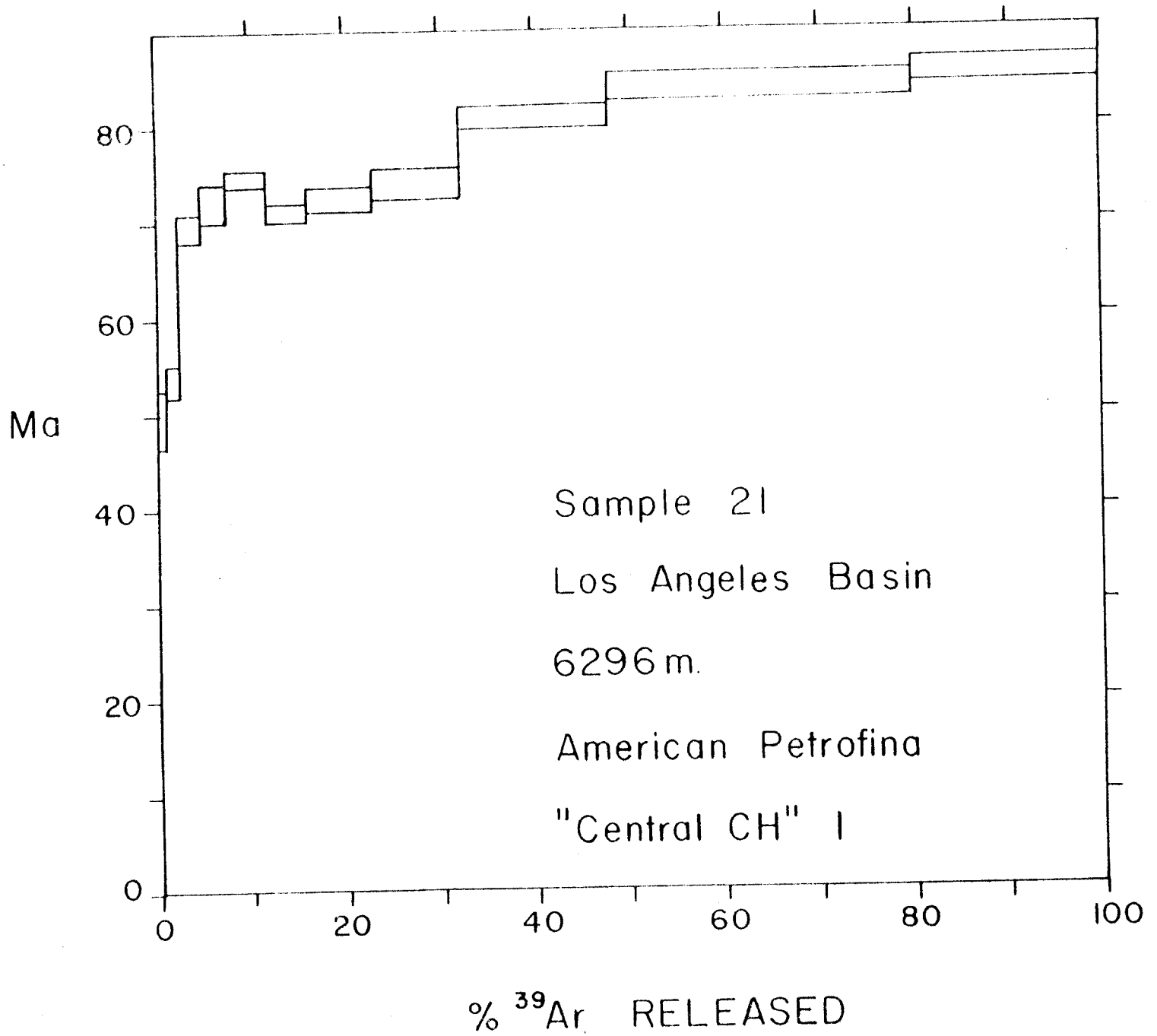
80
60
40
20
0
Ma
Sample 21
Los Angeles Basin
6296 m.
American Petrofina
"Central CH" 1
0
20
40
60
80
100
% ^{39}Ar RELEASED

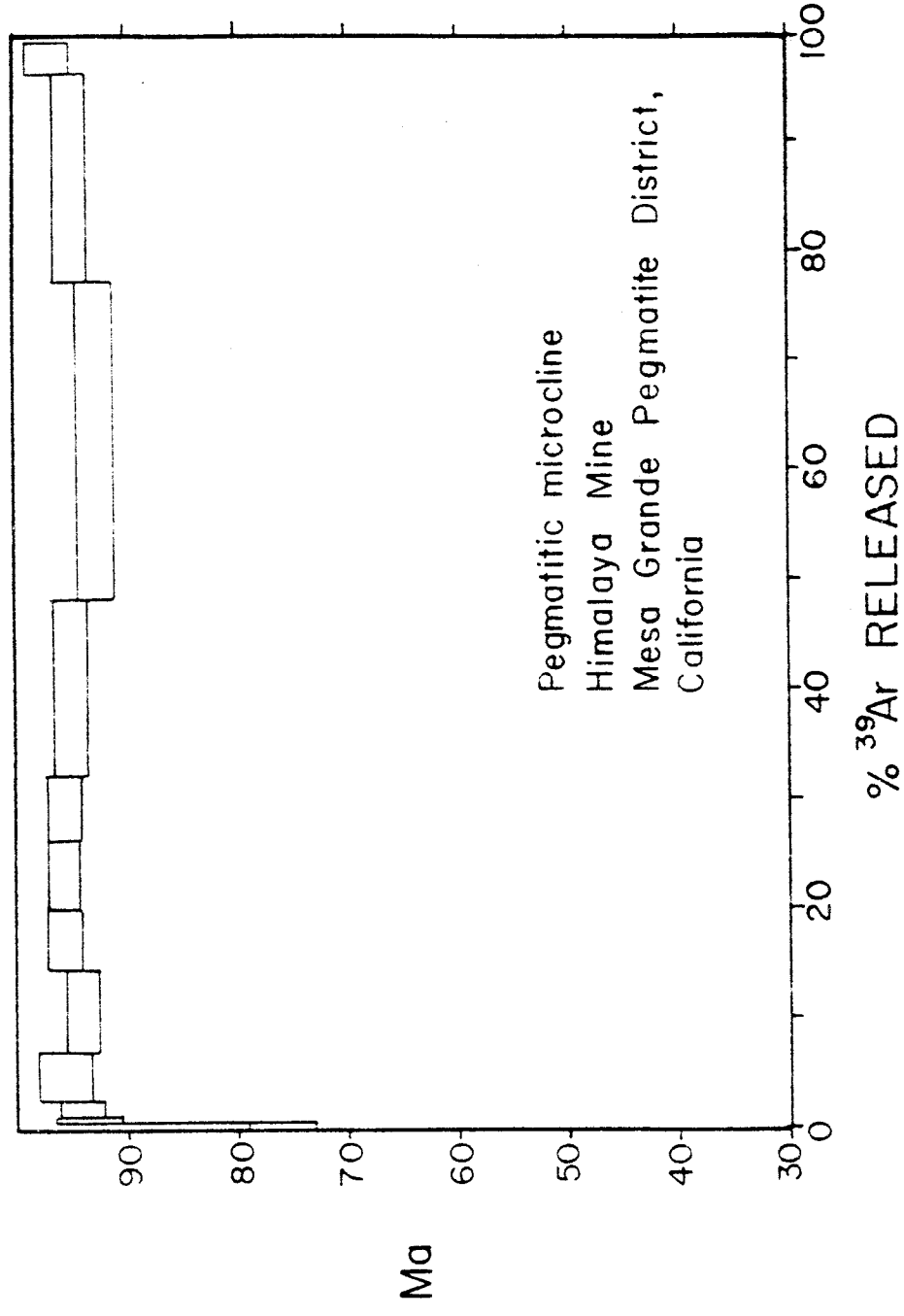
Pegmatitic microcline
Himalaya Mine
Mesa Grande Pegmatite District,
California
Ma
90
80
70
60
50
40
30
0
20
40
60
80
100
% ^{39}Ar RELEASED